AN ABSTRACT OF THE THESIS OF

Madeleine H. Hummel for the degree of Master of Science in Bioengineering presented on November 30, 2021.

Title: Investigating the Hemocompatibility of Blood-Contacting Biomaterials

Abstract approved: _____

Joe E. Baio

Surface-associated thrombosis is a critical concern in medical device development. Current extracorporeal circulation units require systemic anticoagulation to avoid thrombosis, which can cause adverse effects such as thrombocytopenia, hypertriglyceridemia, and hyperkalemia. To address this issue, we combine the technology of polydopamine (PDA) functionalization with slippery liquid infused porous surfaces (SLIPS). PDA readily coats a wide variety of surfaces and can be functionalized via Michael Addition. We functionalized PDA with a thiolated fluoropolymer to form a pseudo self-assembled monolayer (pSAM) that serves as the porous surface component of SLIPS, then added liquid perfluorodecalin to complete the SLIPS coating. We hypothesized that the PDA SLIPS coating provides enhanced hemocompatibility due to its omniphobic properties and composition of compounds currently used in medical applications. The coatings were evaluated for thrombogenicity via quantification of Factor XII (FXII) activation, fibrin formation, and platelet adhesion. In addition to these static test methods, we are developing a flow model to investigate the effect of surface modifications under physiological flow conditions.

Investigating the Hemocompatibility of Blood-Contacting Biomaterials

by
Madeleine H. Hummel

A THESIS

submitted to

Oregon State University

in partial fulfillment of
the requirements for the
degree of

Master of Science

Presented November 30, 2021
Commencement June 2022

Master of Science thesis of Madeleine H. Hummel presented on November 30, 2021.

APPROVED:

Major Professor, representing Bioengineering

Head of the School of Chemical, Biological, and Environmental Engineering

Dean of the Graduate School

I understand that my thesis will become part of the permanent collection of Oregon State University libraries. My signature below authorizes release of my thesis to any reader upon request.

Madeleine H. Hummel, Author

ACKNOWLEDGEMENTS

I would like to thank my advisor, Dr. Joe Baio, and committee members Dr. Kaitlin Fogg, Dr. Adam Higgins, and Dr. Bo Sun for their guidance, advice, and patience over the last couple years. I would also like to thank my lab group and internal and external collaborators for their support and mentorship while working through method development and data collection. Finally, I would like to thank my family and friends for their love, encouragement, and support. I could not have achieved this without them.

TABLE OF CONTENTS

TABLE OF CONTENTS (CONTINUED)

Page

LIST OF FIGURES

Figure Page

LIST OF TABLES

LIST OF APPENDICES

Chapter 1 – Introduction

1.1 Significance

Approximately 60% of babies born with hyperbilirubinemia, a buildup of the neurotoxic compound bilirubin in the blood [1]. Bilirubin is produced during the breakdown of heme through a series of enzymatic reactions [2]. Neonates' livers are often underdeveloped, and blood cell turnover rate is relatively high, leading to the liver not being capable of keeping up with bilirubin production. However, exposure to blue light converts bilirubin to lumirubin, which can be processed and excreted normally by the liver. Therefore, phototherapy treatment involves exposing the patient to blue LEDs to breakdown bilirubin and is usually sufficient for mild cases. The blue light is unable to penetrate the skin and reach blood vessels, so multiple sessions are often required. To avoid neurotoxicity, in situations when bilirubin levels are very high, the bilirubin must be removed more quickly and effectively than what is provided by traditional phototherapy. In the standard treatment for these severe cases, the patient undergoes a high-risk double volume exchange transfusion [3].

The solution to this is photoreactor treatment for severe cases of neonatal jaundice. Previous work has demonstrated the feasibility of photoreactor treatment, which works by removing a small volume of the baby's blood and circulating it through an extracorporeal circuit, where the blood is directly exposed to the same wavelength of blue light used in phototherapy treatments. Extracorporeal circulation units currently marketed for dialysis or extracorporeal membrane oxygenation (ECMO) require systemic anticoagulation, which comes with inherent risks including thrombocytopenia, hypertriglyceridemia, hyperkalemia, and excessive post-operative bleeding [4]. To avoid systemic anticoagulation, the blood-contacting parts of the device must include an antithrombogenic coating. Current approaches for biocompatible coatings include heparinized surfaces and hydrophilic coatings. Surface bound heparin tends to leach over time, resulting in a decrease in activity.

Various hydrophilic coatings have been incorporated into approved medical devices, though still require systemic anticoagulation [5, 6, 7]. We propose that a slippery liquid infused porous surface (SLIPS) coating in conjunction with polydopamine (PDA) modification will provide a foundation for improved blood compatible coatings.

1.2 Coagulation Overview

When a blood vessel sustains damage, the human body quickly recruits a series of proteins, platelets, and other blood clotting factors to the site of injury to form a clot. This is the first step in repairing a damaged vessel and is referred to as the coagulation cascade. The coagulation cascade consists of two major pathways that converge with the activation of thrombin to become the common pathway. Each pathway is complex and all proceed with the same goal: to form a fibrin clot (Figure 1.1). This mechanism is efficient at repairing damage, but also at forming clots on the surface of biomaterials. Clot formation on blood-contacting medical devices can cause various life-threatening conditions including cardiac arrest and stroke. When designing a novel biomaterial or coating for a biomaterial that will be contacting blood, it is important to consider blood compatibility.

Because blood coagulation is complex, demonstrating that a material will not elicit an adverse effect when contacting blood is also complex.

1.2.1 Platelet Adhesion and Activation

Platelets are small, anucleate blood cells that are produced from megakaryocytes. Platelets play a role in homeostasis, thrombosis, angiogenesis, and inflammation [8, 9]. When the blood vessel is damaged, exposed collagen recruits platelets, which adhere to the site of injury, activate, and release granules which promote further aggregation and coagulation. Platelets are the initial plug at the site of injury. In the case of exposure of blood to biomaterials, rapid adsorption of proteins at the interface

recruit and activate platelets. Upon activation, platelets undergo a morphological change. Platelets are discoid in shape while inactive and circulating in the bloodstream.

Once activated, platelets become dendritic and spread in preparation for exocytosis of granule contents. SNARE proteins allow granules to fuse with the open canalicular system on the plasma membrane of the platelet, facilitating exocytosis of granule contents [10]. Platelets contain both α-granules and dense granules, with the former more impactful for coagulation. α-Granules contain coagulation factor V, factor IX, fibrinogen, von Willebrand Factor, β-thromboglobulin, and other chemokines, growth factors, angiogenic factors, integral membrane proteins, and complement system precursors [11, 12, 13].

1.2.2 Contact Activation

The intrinsic coagulation pathway, also called the contact activation pathway, has been shown to become activated when blood contacts biomaterials. In vivo, the extrinsic pathway is favored for coagulation. Patients deficient in intrinsic pathway coagulation factors do not exhibit bleeding disorders. When blood contacts a biomaterial, however, Factor XII can bind to the surface and become activated, leading to a cascade eventually forming a fibrin clot [14].

There are three modes of activation of Factor XII: contact autoactivation, reciprocal activation, and autohydrolysis (Figure 1.2). Contact autoactivation occurs when FXII binds to the surface and undergoes a conformational change, thus activating the protein to FXIIa. Once FXIIa is present, more FXII can be activated through reciprocal activation, which occurs when FXIIa cleaves prekallikrein (PK) from a complex of prekallikrein and high molecular weight kininogen (HMWK) on the surface, producing kallikrein. Kallikrein, in turn, activates FXII. FXII can also undergo a self-amplification process in which FXIIa hydrolyzes FXII to produce

more FXIIa. To further the intrinsic pathway, FXIIa activates FXI, which activates FIX, which activates FX at the start of the common pathway. Autohydrolysis has been shown to be insignificant compared to the other modes of activation because FXIIa has less affinity for FXII than it does for prekallikrein and FXI [15].

1.3 Approaches to Blood Compatible Materials

There are three approaches of surface modification to control thrombus formation: surface passivation, surface activation, and biomimicry [16]. Surface passivation is the engineering of a material such that interactions between the material surface and blood are limited. The goal of surface passivation is to eliminate protein interaction with and adhesion to the material surface [16]. This can be achieved through A general benchmark for protein adhesion to passive surfaces is that less than 1% of a monolayer of protein adheres to the surface [16]. Common examples of surface passivation are binding zwitterionic polymers to material surfaces and inclusion of hydrophilic polymers at the material surface [17, 18, 19]. Surface activation involves binding bioactive molecules to the surface to actively combat coagulation. Heparin is a commonly used clinical systemic anticoagulant that works by binding and activating antithrombin, which in turn inactivates thrombin and prevents thrombus formation [20, 21]. Surface-bound heparin is an example of surface activation, as heparin actively works to prevent thrombin formation. Biomimicry for blood compatibility is the engineering of a surface to mimic the microenvironment of a native blood vessel. This includes porous materials to promote tissue ingrowth and other tissue engineering applications [22].

A recent advance in surface passivation with applications for blood compatibility is the development of slippery liquid-infused porous surfaces (SLIPS) [23]. While many previous liquid-repellent surfaces were inspired by the lotus effect (intricate surface microstructure traps air bubbles to form a composite solid-air interface resulting in superhydrophobicity), SLIPS were designed based on the pitcher plant [23]. Pitcher

plants use their microtextured leaves to trap a layer of liquid on the surface. This liquid causes insects to lose traction on pitcher plant leaves, forcing the insects to slide into the cavity of the pitcher plant that contains digestive juices [24]. SLIPS use similar technology in that they hold onto a liquid layer that repels the liquid of interest. The liquid layer composition is selected such that the liquid is attracted to the substrate and repelled by the contact liquid, in this case blood. The surface is self-healing because the liquid intermediary can flow to cover the surface, including sites of damage [23]. SLIPS were originally cited using inherently porous materials to trap the liquid layer [23]. This technology was then applied to smooth medical-grade materials by modifying the surface with a tethered polymer [7].

SLIPS are of interest for blood-contacting surfaces because the stable liquid intermediary is omniphobic in that it prevents nonspecific adhesion [23,7]. Because protein adsorption is the first step in blood coagulation, preventing blood components from binding will impede thrombus formation. SLIPS have been investigated for blood compatibility previously, primarily using qualitative methods and clotting and platelet adhesion assays [7, 23, 25, 26]. No work has been done on direct activation of FXII on SLIPS surfaces, though Badv et al. hypothesized that their observed prolonged clotting time on SLIPS-coated catheter sheathing was due to reduced activation of the contact system [26]. We believe that constructing a SLIPS coating using a tethered perfluorocarbon and a perfluorodecalin liquid layer will improve blood compatibility and specifically will prevent FXII from activation.

While previous SLIPS coatings have used plasma treatment to graft surface polymers, we are using polydopamine (PDA) to modify the surface. Polydopamine (PDA) is a polymerized biomolecule that has been shown to readily coat a wide variety of surfaces [27]. This technology is based on the mechanism that mussels use to adhere to ships and rocks. Dip coating a material in an aqueous solution of dopamine has been shown to lead to spontaneous deposition of a thin film of polymerized

dopamine. This method has been successfully used on a variety of materials of various surface energies including PTFE, glass, polycarbonate, and gold [27]. Dopamine-coated materials present significant potential for further modification because they can easily be functionalized with thiol- or amine-terminated polymers via Michael addition or Schiff-base formation [28].

Polydopamine coated surfaces can be used in conjunction with SLIPS technology to produce an easily manufactured, self-healing surface. Previous biological analyses of SLIPS have focused primarily on whole blood behavior and cellular toxicity [7, 23, 25, 29]. No studies have been done on the activation of the intrinsic coagulation cascade on SLIPS or on blood compatibility of combination SLIPS dopamine surfaces.

1.4 Hemocompatibility Assays

The most common methods of hemocompatibility analysis are as follows: platelet adhesion and activation, contact activation, clotting time (thrombin or fibrin generation), protein adsorption, and complement system activation. These methods are introduced in the following sections and summarized in Table 1.

1.4.1 Platelet Adhesion and Activation

Platelet adhesion can be measured in several ways including colorimetric assays, scanning electron microscopy (SEM), and radiolabeling. Colorimetric assays for platelet adhesion involve lysing adherent platelets and measuring acid phosphatase or lactate dehydrogenase activity [30, 31, 32]. SEM can be utilized by imaging and counting adherent platelets [33]. Radiolabeling platelets allows for radiological quantification [34]. All of these methods can be utilized to provide platelet counts, with higher platelet counts indicating increased platelet adhesion and decreased hemocompatibility. SEM can also be utilized to quantify platelet activation by

imaging adherent platelets and categorizing them based how spread they are, as spread platelets indicate activation [35, 36].

1.4.2 Contact Activation

FXII activates at the start of the intrinsic coagulation cascade, making it a useful factor to study when quantifying the extent of intrinsic pathway activation. A colorimetric assay can be used to measure the amount of FXIIa via color change. A color change detectable at a wavelength of 405nm is produced when FXIIa acts on its chromogenic substrate. This assay is performed by incubating FXII in buffer or plasma on a surface, then stopping the reaction via kallikrein inhibition. Addition of the chromogenic substrate produces a color change, and the rate of color change can be correlated to the concentration of FXIIa. A higher concentration of FXIIa indicates more contact activation and a less hemocompatible surface.

1.4.3 Clotting Time

Assessment of the time that it takes for this clot to form gives valuable insight into the overall hemocompatibility of a biomaterial. There are three primary clinical tests that evaluate the ability of a patient's blood to clot: prothrombin time (PT), activated partial thromboplastin time (aPTT), and thrombin time (TT). The PT test evaluates the capacity of the extrinsic and common pathways and is performed by adding calcium and thromboplastin to plasma. PT results vary based on the reagents used, so the results are often reported as an International Normalized Ratio (INR). A normal INR is between 0.9 and 1.1, with a higher value indicating deficiencies in the extrinsic or common coagulation pathway. The aPTT test evaluates the intrinsic and common pathways and is performed by incubating a sample with phospholipids and intrinsic pathway activator, then adding calcium to initiate clot formation. Typical aPTT times are 25-37 seconds and a prolonged aPTT indicates deficiencies in the intrinsic or common pathway [37]. TT evaluates the ability of the patient to form fibrin from fibrinogen and is measured by adding exogenous thrombin to plasma [38].

These tests are clinical in nature and have been developed and optimized for high throughput settings. When considering modified surfaces at the lab scale, researchers will often perform a modified PT or aPTT test by incubating recalcified plasma on the surface of interest to evaluate the activation of the extrinsic or intrinsic coagulation pathway, respectively. Colorimetric assays have been utilized to measure thrombin generation. In this method, a color change is produced when thrombin acts on a chromogenic substrate. A faster rate of color change indicates a higher concentration of thrombin, more active coagulation, and therefore a less hemocompatible surface [39]. Another common method of assessing clotting time is a fibrin generation assay based on turbidity [40, 41, 42]. Fibrin generation time can be defined as the time that it takes to reach an absorbance threshold after recalcification. A shorter time to threshold indicates more active coagulation and a less hemocompatible surface.

1.4.4 Protein Adsorption

Protein adsorption is the first event to occur when blood interacts with a biomaterial. Fibrinogen, albumin, and immunoglobulins are found at high concentrations in plasma. Albumin is considered inert and does not promote platelet adhesion and activation. Surface-bound fibrinogen, fibronectin, and von Willebrand factor have been shown to bind to platelets via membrane receptors GPIIb/IIIa and GPIb, causing platelets to adhere to the surface and activate [15]. The rate and quantity of protein adsorption provides insight into hemocompatibility and can provide a deeper explanation of observed trends in other assays. Fibrinogen, von Willebrand factor, and fibronectin are often studied when considering protein adsorption for hemocompatibility purposes because they play roles in platelet adhesion, platelet aggregation, and thrombus stabilization [15]. These particular proteins have specific amino acid sequences (such as RGD) that promote receptor-ligand interactions with platelets [16]. Fibrinogen has been studied extensively and adsorbed fibrinogen conformation has been shown to have a greater effect on platelet adhesion than the amount of adsorbed fibrinogen [43].

The Vroman effect is the phenomena in which high mobility, high concentration proteins adsorb to a surface first, but are then replaced by proteins with higher affinity for the surface over time. An example of the Vroman effect is that fibrinogen adsorbs to a surface first because of its high concentration in plasma but is then replaced over time by HMWK. In this case, HMWK has a high enough affinity for the surface to replace fibrinogen, but this takes time as HMWK has a lower plasma concentration than fibrinogen [16, 43]. Protein adsorption is often quantified by radiolabeling the protein of interest and measuring the radiological signal [44]. This method allows for observation of protein adsorption over time and insight into the Vroman effect.

1.4.5 Complement System Activation

The complement system is composed of approximately 30 proteins that assist the body in distinguishing foreign bodies from native material (Figure 2.3). When activated, proteins in the complement system work to attack foreign bodies. The complement system can be activated through three distinct pathways – the classical pathway, the alternative pathway, and the lectin pathway – all of which converge with the formation of C3 convertase. When C3 is cleaved, it forms C3a and C3b. C3b helps form C5 convertase, which cleaves C5 into C5a and C5b. C5b initiates the membrane attack complex and C5b-9, which is also referred to as the terminal complement complex (TCC) [45, 46]. Formation of C3a, C5b, and C5b-9 represent critical steps in complement system activation and are often quantified when complement system activation is of concern. Off-the-shelf ELISA kits are available for these proteins. Higher concentrations of complement system components signifies more significant complement system activation and therefore a less hemocompatible surface.

We propose that a SLIPS coating via PDA modification will provide a basis for a hemocompatible coating intended for extracorporeal circulation units due to limited activation of coagulation factor XII and extended plasma clotting time.

1.5 References

1. S. Ullah, K. Rahman, and M. Hedayati, “Hyperbilirubinemia in Neonates: Types, Causes, Clinical Examinations, Preventive Measures and Treatments: A Narrative Review Article,” *Iran J Public Health*, vol. 45, no. 5, pp. 558–568, May 2016.

2. L. Ngashangva, V. Bachu, and P. Goswami, “Development of new methods for determination of bilirubin,” *Journal of Pharmaceutical and Biomedical Analysis*, vol. 162, pp. 272–285, Jan. 2019, doi: 10.1016/j.jpba.2018.09.034.

3. N. Bujandric and J. Grujic, “Exchange Transfusion for Severe Neonatal Hyperbilirubinemia: 17 Years’ Experience from Vojvodina, Serbia,” *Indian J Hematol Blood Transfus*, vol. 32, no. 2, pp. 208–214, Jun. 2016, doi: 10.1007/s12288-015-0534-1.

4. R. E. Cronin and R. F. Reilly, “Unfractionated Heparin for Hemodialysis: Still the Best Option: UNFRACTIONATED HEPARIN FOR HEMODIALYSIS,” *Seminars in Dialysis*, vol. 23, no. 5, pp. 510–515, Sep. 2010, doi: 10.1111/j.1525-139X.2010.00770.x.

5. D. A. Palanzo *et al.*, “Effect of Carmeda BioActive Surface coating versus Trillium Biopassive Surface coating of the oxygenator on circulating platelet count drop during cardiopulmonary bypass,” *Perfusion*, vol. 16, no. 4, pp. 279–283, Jul. 2001, doi: 10.1177/026765910101600403.

6. A. S. Thiara *et al.*, “Comparable biocompatibility of Phisio- and Bioline-coated cardiopulmonary bypass circuits indicated by the inflammatory response,” *Perfusion*, vol. 25, no. 1, pp. 9–16, Jan. 2010, doi: 10.1177/0267659110362822.

7. D. C. Leslie *et al.*, “A bioinspired omniphobic surface coating on medical devices prevents thrombosis and biofouling,” *Nature Biotechnology*, vol. 32, no. 11, Art. no. 11, Nov. 2014, doi: 10.1038/nbt.3020.

8. P. Blair and R. Flaumenhaft, “Platelet α–granules: Basic biology and clinical correlates,” *Blood Rev*, vol. 23, no. 4, pp. 177–189, Jul. 2009, doi: 10.1016/j.blre.2009.04.001.

9. M. M. Frojmovic and J. G. Milton, “Human platelet size, shape, and related functions in health and disease.,” *Physiological Reviews*, vol. 62, no. 1, pp. 185–261, Jan. 1982, doi: 10.1152/physrev.1982.62.1.185.

10. J. G. White and C. C. Clawson, “The surface-connected canalicular system of blood platelets--a fenestrated membrane system.,” *Am J Pathol*, vol. 101, no. 2, pp. 353–364, Nov. 1980.

11. J. L. Fitch-Tewfik and R. Flaumenhaft, “Platelet Granule Exocytosis: A Comparison with Chromaffin Cells,” *Front Endocrinol (Lausanne)*, vol. 4, Jun. 2013, doi: 10.3389/fendo.2013.00077.

12. J. E. Rothman and L. Orci, “Molecular dissection of the secretory pathway,” *Nature*, vol. 355, no. 6359, pp. 409–415, Jan. 1992, doi: 10.1038/355409a0.

13. “SNAP receptors implicated in vesicle targeting and fusion | Nature.” https://www.nature.com/articles/362318a0 (accessed Nov. 18, 2021).

14. C. Sperling, M. Fischer, M. F. Maitz, and C. Werner, “Blood coagulation on biomaterials requires the combination of distinct activation processes,” *Biomaterials*, vol. 30, no. 27, pp. 4447–4456, Sep. 2009, doi: 10.1016/j.biomaterials.2009.05.044.

15. L.-C. Xu, J. W. Bauer, and C. A. Siedlecki, “Proteins, platelets, and blood coagulation at biomaterial interfaces,” *Colloids and Surfaces B: Biointerfaces*, vol. 124, pp. 49–68, Dec. 2014, doi: 10.1016/j.colsurfb.2014.09.040.

16. X. Liu *et al.*, “Blood compatible materials: state of the art,” *J. Mater. Chem. B*, vol. 2, no. 35, pp. 5718–5738, Aug. 2014, doi: 10.1039/C4TB00881B.

17. P.-S. Liu *et al.*, “Grafting of Zwitterion from Cellulose Membranes via ATRP for Improving Blood Compatibility,” *Biomacromolecules*, vol. 10, no. 10, pp. 2809–2816, Oct. 2009, doi: 10.1021/bm9006503.

18. Y. Chang, W.-J. Chang, Y.-J. Shih, T.-C. Wei, and G.-H. Hsiue, “Zwitterionic Sulfobetaine-Grafted Poly(vinylidene fluoride) Membrane with Highly Effective Blood Compatibility via Atmospheric Plasma-Induced Surface Copolymerization,” *ACS Appl. Mater. Interfaces*, vol. 3, no. 4, pp. 1228–1237, Apr. 2011, doi: 10.1021/am200055k.

19. K. Ishihara, T. Ueda, and N. Nakabayashi, “Preparation of Phospholipid Polymers and Their Properties as Polymer Hydrogel Membranes,” *Polymer Journal*, vol. 22, no. 5, Art. no. 5, May 1990, doi: 10.1295/polymj.22.355.

20. R. Carrell, R. Skinner, M. Wardell, and J. Whisstock, “Antithrombin and heparin,” *Molecular Medicine Today*, vol. 1, no. 5, pp. 226–231, Aug. 1995, doi: 10.1016/S1357-4310(95)91494-3.

21. L. Jin, J. P. Abrahams, R. Skinner, M. Petitou, R. N. Pike, and R. W. Carrell, “The anticoagulant activation of antithrombin by heparin,” *Proc Natl Acad Sci U S A*, vol. 94, no. 26, pp. 14683–14688, Dec. 1997.

22. L. Bordenave, M. Rémy-Zolghadri, P. Fernandez, R. Bareille, and D. Midy, “Clinical performance of vascular grafts lined with endothelial cells,” *Endothelium*, vol. 6, no. 4, pp. 267–275, 1999, doi: 10.3109/10623329909078494.

23. T.-S. Wong *et al.*, “Bioinspired self-repairing slippery surfaces with pressure-stable omniphobicity,” *Nature*, vol. 477, no. 7365, Art. no. 7365, Sep. 2011, doi: 10.1038/nature10447.

24. U. Bauer and W. Federle, “The insect-trapping rim of Nepenthes pitchers,” *Plant Signal Behav*, vol. 4, no. 11, pp. 1019–1023, Nov. 2009.

25. K. Manabe, K.-H. Kyung, and S. Shiratori, “Biocompatible Slippery Fluid-Infused Films Composed of Chitosan and Alginate via Layer-by-Layer Self-Assembly and Their Antithrombogenicity,” *ACS Appl. Mater. Interfaces*, vol. 7, no. 8, pp. 4763–4771, Mar. 2015, doi: 10.1021/am508393n.

26. M. Badv, I. H. Jaffer, J. I. Weitz, and T. F. Didar, “An omniphobic lubricant-infused coating produced by chemical vapor deposition of hydrophobic organosilanes attenuates clotting on catheter surfaces,” *Scientific Reports (Nature Publisher Group)*, vol. 7, pp. 1–10, Sep. 2017, doi: http://dx.doi.org.ezproxy.proxy.library.oregonstate.edu/10.1038/s41598-017-12149-1.

27. H. Lee, S. M. Dellatore, W. M. Miller, and P. B. Messersmith, “Mussel-Inspired Surface Chemistry for Multifunctional Coatings,” *Science*, vol. 318, no. 5849, pp. 426–430, Oct. 2007, doi: 10.1126/science.1147241.

28. C.-Y. Liu and C.-J. Huang, “Functionalization of Polydopamine via the Aza-Michael Reaction for Antimicrobial Interfaces,” *Langmuir*, vol. 32, no. 19, pp. 5019–5028, May 2016, doi: 10.1021/acs.langmuir.6b00990.

29. C. Howell, A. Grinthal, S. Sunny, M. Aizenberg, and J. Aizenberg, “Designing Liquid-Infused Surfaces for Medical Applications: A Review,”

Advanced Materials, vol. 30, no. 50, p. 1802724, 2018, doi: https://doi.org/10.1002/adma.201802724.

30. M. Vaníčková, J. Suttnar, and J. E. Dyr, "The adhesion of blood platelets on fibrinogen surface: Comparison of two biochemical microplate assays," *Platelets*, vol. 17, no. 7, pp. 470–476, Nov. 2006, doi: 10.1080/09537100600758875.

31. Y. Tamada, E. A. Kulik, and Y. Ikada, "Simple method for platelet counting," *Biomaterials*, vol. 16, no. 3, pp. 259–261, Feb. 1995, doi: 10.1016/0142-9612(95)92126-q.

32. P. Bellavite *et al.*, "A colorimetric method for the measurement of platelet adhesion in microtiter plates," *Anal Biochem*, vol. 216, no. 2, pp. 444–450, Feb. 1994, doi: 10.1006/abio.1994.1066.

33. L. J. Suggs, J. L. West, and A. G. Mikos, "Platelet adhesion on a bioresorbable poly(propylene fumarate-co-ethylene glycol) copolymer," *Biomaterials*, vol. 20, no. 7, pp. 683–690, Apr. 1999, doi: 10.1016/s0142-9612(98)00226-9.

34. K. D. Curwen, H. Y. Kim, M. Vazquez, R. I. Handin, and M. A. Gimbrone, "Platelet adhesion to cultured vascular endothelial cells. A quantitative monolayer adhesion assay," *J Lab Clin Med*, vol. 100, no. 3, pp. 425–436, Sep. 1982.

35. S. L. Goodman, "Sheep, pig, and human platelet-material interactions with model cardiovascular biomaterials," *J Biomed Mater Res*, vol. 45, no. 3, pp. 240–250, Jun. 1999, doi: 10.1002/(sici)1097-4636(19990605)45:3<240::aid-jbm12>3.0.co;2-c.

36. R. Khalifehzadeh, W. Ciridon, and B. D. Ratner, "Surface fluorination of polylactide as a path to improve platelet associated hemocompatibility," *Acta Biomaterialia*, vol. 78, pp. 23–35, Sep. 2018, doi: 10.1016/j.actbio.2018.07.042.

37. A. H. Kamal, A. Tefferi, and R. K. Pruthi, "How to interpret and pursue an abnormal prothrombin time, activated partial thromboplastin time, and bleeding time in adults," *Mayo Clinic Proceedings*, vol. 82, no. 7, pp. 864-, Jul. 2007.

38. M. M. Flanders, R. Crist, and G. M. Rodgers, “Comparison of Five Thrombin Time Reagents,” *Clin Chem*, vol. 49, no. 1, pp. 169–172, Jan. 2003, doi: 10.1373/49.1.169.

39. K. N. J. Stevens, Y. B. J. Aldenhoff, F. H. van der Veen, J. G. Maessen, and L. H. Koole, “Bioengineering of Improved Biomaterials Coatings for Extracorporeal Circulation Requires Extended Observation of Blood-Biomaterial Interaction under Flow,” *J Biomed Biotechnol*, vol. 2007, 2007, doi: 10.1155/2007/29464.

40. N. M. Bates, C. Puy, P. L. Jurney, O. J. T. McCarty, and M. T. Hinds, “Evaluation of the Effect of Crosslinking Method of Poly(Vinyl Alcohol) Hydrogels on Thrombogenicity,” *Cardiovasc Eng Tech*, vol. 11, no. 4, pp. 448–455, Aug. 2020, doi: 10.1007/s13239-020-00474-y.

41. K. N. Sask, W. G. McClung, L. R. Berry, A. K. C. Chan, and J. L. Brash, “Immobilization of an antithrombin–heparin complex on gold: Anticoagulant properties and platelet interactions,” *Acta Biomaterialia*, vol. 7, no. 5, pp. 2029–2034, May 2011, doi: 10.1016/j.actbio.2011.01.031.

42. S. A. Smith and J. H. Morrissey, “Polyphosphate enhances fibrin clot structure,” *Blood*, vol. 112, no. 7, pp. 2810–2816, Oct. 2008, doi: 10.1182/blood-2008-03-145755.

43. T. A. Horbett, “Fibrinogen adsorption to biomaterials,” *J Biomed Mater Res A*, vol. 106, no. 10, pp. 2777–2788, Oct. 2018, doi: 10.1002/jbm.a.36460.

44. T. A. Horbett and P. K. Weathersby, “Adsorption of proteins from plasma to a series of hydrophilic-hydrophobic copolymers. I. Analysis with the in situ radioiodination technique,” *Journal of Biomedical Materials Research*, vol. 15, no. 3, pp. 403–423, 1981, doi: 10.1002/jbm.820150311.

45. M. Weber *et al.*, “Blood-Contacting Biomaterials: In Vitro Evaluation of the Hemocompatibility,” *Front Bioeng Biotechnol*, vol. 6, Jul. 2018, doi: 10.3389/fbioe.2018.00099.

46. L. M. Szott, M. J. Stein, B. D. Ratner, and T. A. Horbett, “Complement activation on poly(ethylene oxide)-like RFGD-deposited surfaces,” *J Biomed Mater Res A*, vol. 96, no. 1, pp. 150–161, Jan. 2011, doi: 10.1002/jbm.a.32954.

47. M. M. Markiewski, B. Nilsson, K. Nilsson Ekdahl, T. E. Mollnes, and J. D. Lambris, “Complement and coagulation: strangers or partners in crime?,” *Trends in Immunology*, vol. 28, no. 4, pp. 184–192, Apr. 2007, doi: 10.1016/j.it.2007.02.006.

Assay	Analytical Method	Measured Variable	Interpretation	Ref.
Platelet Adhesion	Colorimetric Assay	Color change produced by LDH, ACP action on chromogenic substrate	Faster rate of color change indicates higher LDH, ACP concentration → more platelets adhered, less hemocompatible	Vaníčková 2006, Tamada 1995, Bellavite 1994
	SEM	Platelet count via imaging	Higher platelet count indicates lower hemocompatibility	Suggs 1999
	Radiolabeling	Radiological activity	Platelets radiolabeled; higher radiological signal indicates more platelets adhered, less hemocompatible	Curwen 1982
Platelet Activation	SEM	Platelet counts via imaging	Categorize and count platelets by morphology; higher ratio of spread to discoid platelets indicates more platelet activation, lower hemocompatibility	Goodman 1999, Khalifazadeh 2018
Contact Activation	Colorimetric Assay	Color change produced by FXIIa action on	Faster rate of color change indicates higher FXIIa concentration → more	Bäck 2010, Bates 2020

		chromogenic substrate	intrinsic activation, less hemocompatible	
Clotting Time	Colorimetric Assay	Color change produced by thrombin action on chromogenic substrate	Faster rate of color change indicates higher thrombin concentration → less hemocompatible	Aldenhoff 1997, Stevens 2007
	Turbidimetry	Presence of fibrin	Time to threshold indicates clotting time; shorter time → less hemocompatible	Bates 2020, Sask 2011
Protein Adsorption	Radiolabeling	Radiological activity	Higher radiological signal indicates more proteins adsorbed to surface	Helkamp 1960, Horbett 1981
Complement System	ELISA	C3a, C5b, C5b-9 concentration	Higher concentration indicates more complement system activation	Szott 2011

Table 1. Summary of blood compatibility assays.

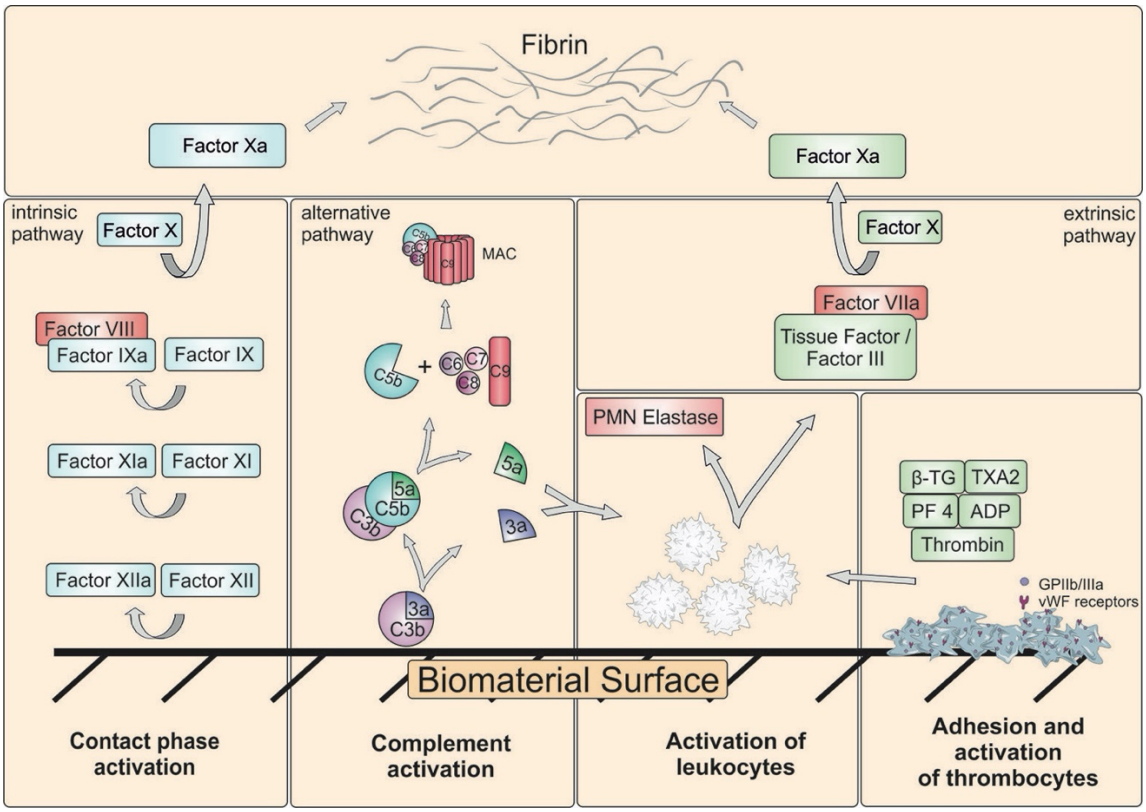

Figure 1.1. Schematic of blood reactions at a biointerface (figure from Weber *et al.* 2018 [45]). Contact activation, complement system activation, leukocytes, thrombocytes, and the extrinsic pathway all contribute to the formation of a crosslinked fibrin clot.

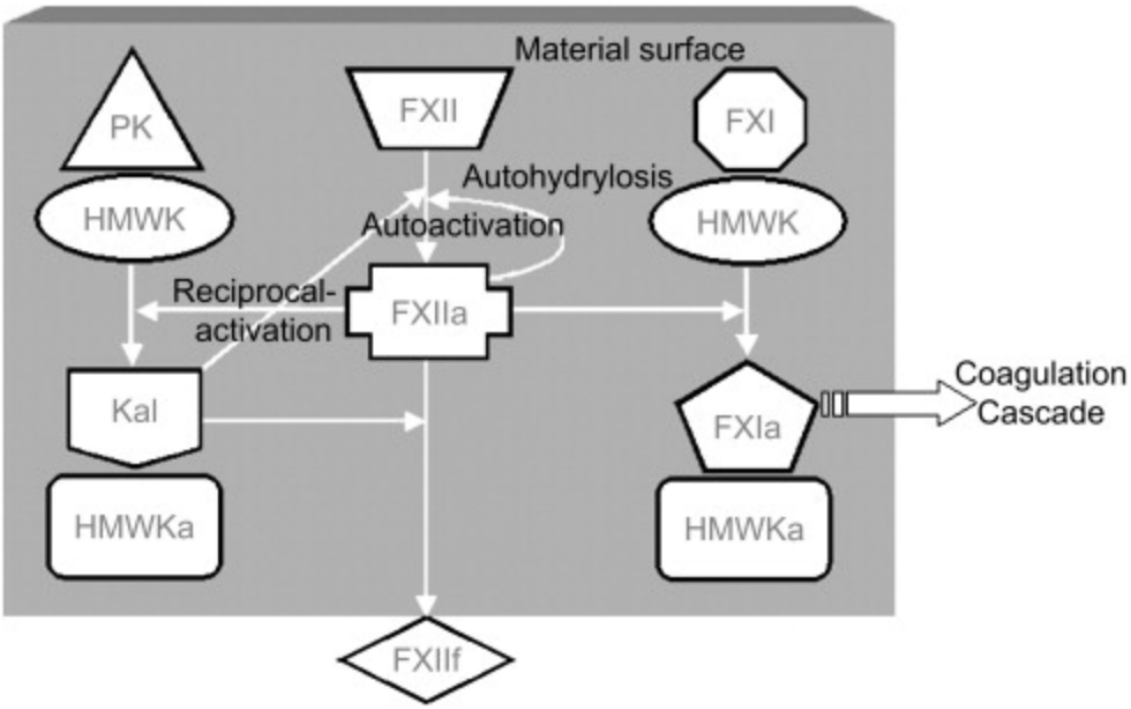

Figure 1.2. Schematic of FXII activation. Contact autoactivation occurs when FXII undergoes a conformational change when bound to a surface. Reciprocal activation occurs when FXII cleaves kallikrein from a complex of PK and HMWK. Autohydrolysis occurs when FXIIa hydrolyzes FXII into FXIIa (figure from Xu *et al.* 2014 [5]).

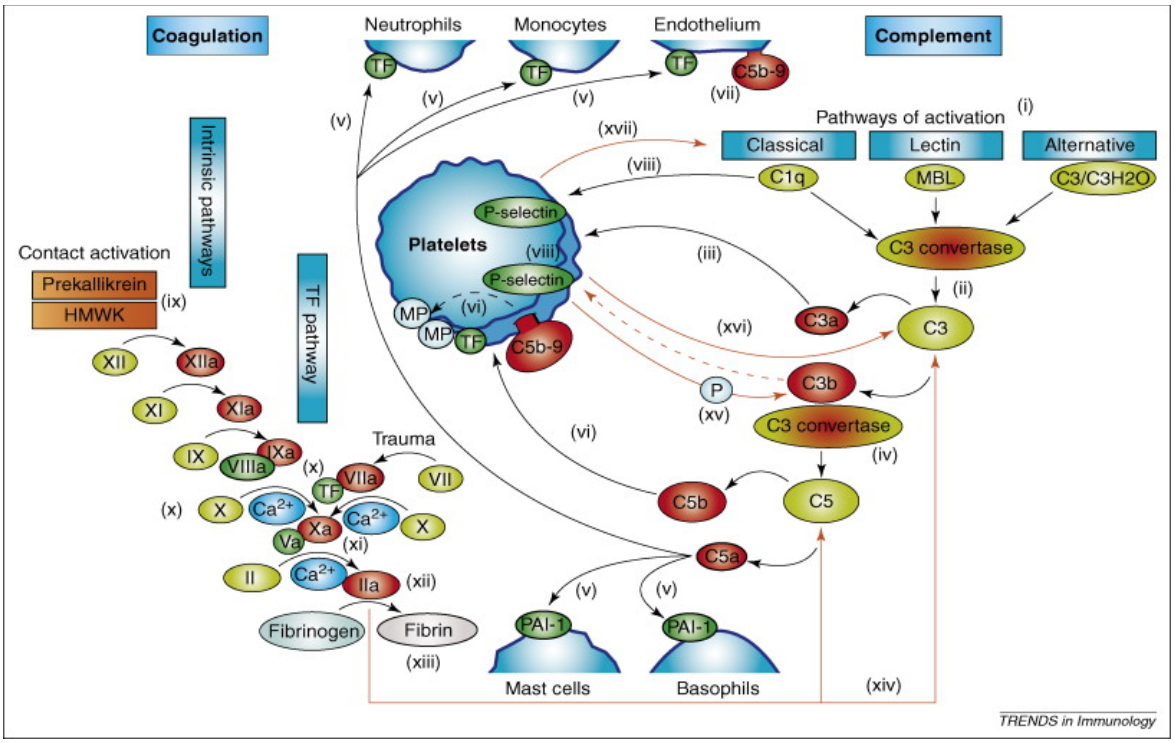

Figure 1.3. Schematic of complement system and interplay with coagulation cascade. The three pathways of contact system activation (classical, lectin, and alternative) aid in the production of C3a, which interacts with platelets (Figure from Markiewski *et al.* 2007 [47]).

Chapter 2 – Methods

2.1 UV-Vis Absorption Spectroscopy

UV-Vis absorption spectroscopy is a common laboratory technique that utilizes a light source, monochromator, and detector to determine the amount of light that a sample absorbs (Figure 2.1). This can be used to determine the amount of a specific compound in solution. Microplate readers operate according to the same principles as a spectrophotometer but allow for higher throughput analysis due to their capability to read multiple wells in succession compared to a single cuvette. Plate readers are also equipped with more advanced analytical techniques including kinetic readings and integrated fluorescence and luminescence capabilities. Absorption is defined as the process of diminishing light due to excitation of molecules in a sample and is measured as the logarithm of the ratio of incident light intensity to transmitted light intensity. Absorbance is described by the Lambert-Beer Law (Eq. 2.1).

$$A = \log\frac{I_0}{I} = \varepsilon bC \quad \text{(Eq. 2.1)}$$

Where A is the absorbance, I_0 is the incident light intensity, I is the measured light intensity after passing through the sample, is the molar absorption coefficient, b is the path length of light through the sample, and C is the concentration of the absorbing species [1]. The Lambert-Beer Law is valid only under strict experimental conditions including: (i) monochromatic light, (ii) homogeneous sample solution, (iii) absence of light scattering in the sample, (iv) absence of photochemical reactions in the sample, and (v) non-fluorescing sample [2]. In general, experiments should be designed such that the absorbance is between 0 and 2 because that is the range where the Lambert-Beer Law assumptions are valid.

The wavelength of the light source for most instruments can range between 200 and 1000nm and is tunable to within 1-2nm [2]. This wavelength range encompasses the entirety of the visible light spectrum and some UV and IR light.

When the conditions for the Lambert-Beer Law are met, absorbance is directly proportional to concentration. A standard curve can be generated by measuring and plotting the absorbance of solutions with well-defined concentrations. The slope of the resulting line will be the product of ε and b. When ε and b are held constant (i.e., sample constituents, preparation, and instrumentation remain the same), the standard curve can then be used to convert measured absorbance values to concentration for samples of unknown concentration.

Often in biochemistry, samples do not naturally produce color in the UV-Vis spectrum. In these cases, a measurable color change is produced by a chromogenic substrate. [3, 4]. Chromogenic substrates are sequences of amino acids attached to a chromophore that can be used to measure enzymatic activity. When bound, the chromophore is colorless, but when cleaved, it produces color. The sequence of amino acids in the chromogenic substrate is selected to signal to the enzyme of interest where to cut (Figure 2.2). When the enzyme cleaves the chromophore from the amino acid sequence, a color change is produced. In the case of FXIIa, the enzyme cleaves paranitroaniline from a sequence of amino acids (proline, phenylalanine, arginine), causing paranitroanaline to change from colorless to yellow. The rate of color change is dependent on the concentration of enzyme. The Lambert-Beer Law can be applied to kinetic experiments to measure the activity of an enzyme (Eq. 2.2).

$$\frac{A}{t} = \varepsilon b \frac{C}{t} \quad \text{(Eq. 2.2)}$$

The change in absorbance over time is directly proportional to the change in concentration of the chromophore over time, which is directly proportional to enzyme concentration.

2.1.1 Colorimetric Assay for Activated Human FXII

There are three distinct methods of activation of FXII: contact autoactivation, reciprocal activation, and autohydrolysis. Contact autoactivation occurs when FXII undergoes a conformational change when bound to a surface. Reciprocal activation occurs when FXII cleaves kallikrein from a complex of PK and HMWK. Autohydrolysis occurs when FXIIa hydrolyzes FXII into FXIIa, though is considered insignificant compared to autoactivation and reciprocal activation [5, 6]. Figure 2.3 depicts these distinct pathways. Higher concentrations of FXIIa indicate more activation of the intrinsic coagulation cascade, suggesting increased risk of thrombosis.

A colorimetric assay for FXIIa can be used to quantify surface associated FXII activation. FXII activation can be measured in buffer with FXII the only zymogen present [3, 7] in buffer with FXII and cofactors pre-kallikrein and high molecular weight kininogen [3, 8], or in plasma [7, 9]. When FXIIa is quantified after exposing a surface to inactive FXII in buffer, only autoactivation and autohydrolysis are measured. When quantified from FXII, PK and HMWK in buffer, FXIIa concentration represents FXII activated from a combination of autoactivation, reciprocal activation, and autohydrolysis. Though less common, FXIIa can also be quantified in plasma exposed to biomaterial surfaces [7, 9]. This introduces factors such as competitive binding and other interactions between components of the coagulation cascade.

To perform a colorimetric assay for FXII, first the wells of a non-treated polystyrene 96-well plate are coated with bovine serum albumin (BSA). BSA readily coats

polystyrene and prevents FXII from both binding and activating at the well surface. The result of the BSA blocking step is that the measured FXIIa is FXII activated by the experimental surface. After blocking wells with BSA, 5mm diameter experimental surfaces placed inside to wells. Next, the FXII solution (FXII in buffer or FXII, PK and HMWK in buffer) is added and allowed to incubate in the wells at 37°C for 1 hour. After is incubation step, the protein solution is quenched with soybean trypsin inhibitor (SBTI) and chromogenic substrate S-2302 is added. Both FXIIa and kallikrein act on S-2302, so SBTI is included to inhibit kallikrein and ensure all measured color change is a result of FXIIa. The absorbance is measured every minute for one hour at 405nm (Figure 2.4).

The resultant data of absorbance can be plotted versus experimental time and in most cases the is linear. Using a standard curve generated from known concentrations of FXIIa, the absorbance over time can be converted to enzyme concentration. A MATLAB code (Appendix A) was developed to calculate FXIIa concentration from raw absorbance and time data.

2.2 Turbidimetry

Turbidimetry is the study of light scattering and absorption due to particles suspended in solution. Absorbance spectroscopy is utilized to study photon behavior, but the Lambert-Beer Law is not valid because the solution is not homogeneous. Turbidity analysis is common for environmental science and engineering applications, specifically water analysis to identify and quantify contaminant concentrations [10]. Specific instrumentation exists for this application and operates using similar technology to spectrophotometers, but with a tunable backscatter detector (Figure 2.5).

Turbidity analysis can be used to study clot formation kinetics [3, 11, 12]. As fibrin is formed from fibrinogen, the solution becomes more turbid. This change in turbidity can be measured using absorbance spectroscopy, most commonly at 405nm [3, 11]. The absorbance versus time curve from fibrin generation data is S-shaped. While there is no standardized method for determining fibrin generation time, three methods for processing turbidimetric fibrin generation data are as follows: (i) time to reach a 5% increase over the baseline absorbance [3], (ii) time to half the maximum absorbance (Langer 1988), (iii) intersection between line fitted to steepest part of curve and baseline [11].

To perform the turbidimetric assay for fibrin generation, wells of a non-treated polystyrene 96-well plate must be blocked with BSA. Surfaces were added to the wells. Plasma, buffer, and calcium chloride were added to each well and the absorbance was measured over time at 405nm in a plate reader (Figure 2.6). To prevent premature coagulation, sodium citrate is added to the plasma at the time of the blood draw. Calcium is required for various steps in the coagulation cascade including the activation of thrombin and sodium citrate prevents coagulation by chelating calcium [13]. The addition of calcium chloride overcomes the effect of sodium citrate, allowing for coagulation to proceed.

In these experiments, we defined the fibrin generation time as the time to reach a 5% increase over baseline absorbance [3]. The 5% threshold is sufficient to overcome the noise floor of the data. The baseline was defined as the average absorbance of time points 2 through n-1, where n is the time point where the absorbance begins to visibly increase for the sample that is fastest to clot. A MATLAB code (Appendix B) was developed to take the inputs of raw absorbance and time data and baseline start and stop times and return output plots with the raw data curve, threshold, and interpolated fibrin generation time. The code also outputs a table with the calculated fibrin

generation time for each sample. Linear interpolation between the time points on either side of the threshold was used to calculate the fibrin generation time.

2.3 Scanning Electron Microscopy

A scanning electron microscope (SEM) scans a surface with a beam of electrons focused through a series of apertures and electromagnetic lenses. SEMs operate in a vacuum. When electrons interact with the sample surface, five events can occur: (i) emission of secondary electrons, (ii) backscattered primary electrons, (iii) absorption of electrons, (iv) emission of x-rays from the sample, and (v) emission of photons from the sample [14]. A scintillation or solid-state detector is used to count backscattered and secondary electrons, and this signal is amplified and converted to an electrical signal that represents an image of the surface topography. The number of backscattered, secondary, and absorbed electrons at a given location depend on the topography at that location. A magnification of 300,000x and a resolution of 1nm can be achieved under optimal conditions, though lower magnification and resolution are sufficient for most applications.

SEM samples imaged under high vacuum must be vacuum compatible, dry, and electrically conductive. Because biological samples tend to have high water content and are not electrically conductive, specific sample preparation procedures must be followed. After preparing the sample to be imaged, it must be fixed using a cross-linking agent such as glutaraldehyde to preserve the condition of the sample. Next, samples are dehydrated in a series of ethanol rinses then critical point dried. Samples are then mounted to stubs and sputter coated in gold/palladium. The resulting sample has preserved its state but is dry and electrically conductive as required by the SEM [14].

All experiments were performed on a Quanta 600 FEG SEM at the Oregon State University Electron Microscopy Facility. The resolution of this instrument can reach

1.7nm. Samples were imaged at a maximum of 40,000x magnification for a horizontal field width (HFW) of 6.4um.

2.3.1 Scanning Electron Microscopy of Clotted Plasma

Clot morphology can give insight into the thrombogenicity of a surface [15]. Clots with larger diameter fibers and less dense networks indicate clots that are easier to break down and therefore less stable [15]. To investigate the thrombogenicity of surfaces, plasma can be clotted on a surface then imaged using SEM. An image processing software such as ImageJ can be used to measure fiber diameter and clot density. Clot density can be quantified by drawing an arbitrary line of fixed length then counting the number of fibers that cross the line [15].

Fibrin networks for SEM are often prepared in a purified system [11, 15, 16]. A wide variety of proteins play roles in clot formation, so we prepared clots for SEM using platelet-poor plasma. The process for preparing clots for SEM was the same as preparing clots for turbidimetric analysis.

2.3.2 Scanning Electron Microscopy for Platelet Adhesion and Activation

Platelet adhesion is an established metric for surface thrombogenicity [3, 12, 17, 18, 19]. When platelets adhere to a surface and activate, granules that promote coagulation are secreted. Therefore, decreased adherent and activated platelet counts indicated improved hemocompatibility of a surface. To prepare samples, platelets in neat buffer are incubated on a surface. The surface is then rinsed to remove all non-adherent material, then fixed, dehydrated, and sputter coated to prepare for imaging (Figure 2.7). To quantify platelet adhesion, the total platelets in a given surface area are counted. To quantify platelet activation, platelets area was measured using ImageJ.

2.4 Biological Material Sourcing and Processing

FXIIa assays were performed in HEPES buffered saline with BSA. Purified human FXII, PK and HMWK were purchased from Enzyme Research Laboratories. Turbidimetry and clot morphology experiments were performed using purchased human pooled plasma (Sigma) and single donor platelet poor plasma (PPP) from fresh human blood samples. Platelet studies were performed in purified platelet solutions from fresh human blood samples.

Blood samples were collected from volunteers at Oregon State University Student Health Services (Corvallis, OR) in accordance with an approved IRB. These samples were processed by the method established by McCarty *et al*. [20]. Blood was collected into a syringe containing 3.8% sodium citrate at a ratio one part sodium citrate to 10 parts blood. Acid-citrate-dextrose (ACD) was added to the blood at a 1:10 ratio. Blood samples were transferred into 15ml centrifuge tubes and centrifuged at 200g for 20 minutes at room temperature. This separates the blood into three layers: erythrocytes at the bottom, a thin "buffy coat" of white blood cells in the middle, and platelet rich plasma at the top. Supernatant platelet rich plasma was transferred to a new tube and prostaglandin I2 was added to inhibit platelet activation. The plasma was centrifuged at 1000g for 10 minutes at room temperature to pellet the platelets. The supernatant platelet poor plasma was decanted and used within 12 hours for clotting assays. The pelleted platelets were resuspended in Tyrode's buffer and ACD and prostaglandin I2 was again added to inhibit platelet activation during centrifugation. The platelet solution was centrifuged at 1000g for 10 minutes at room temperature and the supernatant was discarded. Pelleted platelets were resuspended in Tyrode's buffer to a volume of 10% of the initial blood draw. Platelets were diluted 1:1000 and counted using a hemocytometer. The platelet solution was then diluted to the desired concentration (Figure 2.8).

2.5 References

1. D. F. Swinehart, "The Beer-Lambert Law," p. 3.

2. W. Mäntele and E. Deniz, “UV–VIS absorption spectroscopy: Lambert-Beer reloaded,” *Spectrochimica Acta Part A: Molecular and Biomolecular Spectroscopy*, vol. 173, pp. 965–968, Feb. 2017, doi: 10.1016/j.saa.2016.09.037.

3. N. M. Bates, C. Puy, P. L. Jurney, O. J. T. McCarty, and M. T. Hinds, “Evaluation of the Effect of Crosslinking Method of Poly(Vinyl Alcohol) Hydrogels on Thrombogenicity,” *Cardiovasc Eng Tech*, vol. 11, no. 4, pp. 448–455, Aug. 2020, doi: 10.1007/s13239-020-00474-y.

4. K. N. J. Stevens, Y. B. J. Aldenhoff, F. H. van der Veen, J. G. Maessen, and L. H. Koole, “Bioengineering of Improved Biomaterials Coatings for Extracorporeal Circulation Requires Extended Observation of Blood-Biomaterial Interaction under Flow,” *J Biomed Biotechnol*, vol. 2007, 2007, doi: 10.1155/2007/29464.

5. L.-C. Xu, J. W. Bauer, and C. A. Siedlecki, “Proteins, platelets, and blood coagulation at biomaterial interfaces,” *Colloids and Surfaces B: Biointerfaces*, vol. 124, pp. 49–68, Dec. 2014, doi: 10.1016/j.colsurfb.2014.09.040.

6. M. Schapira *et al.*, “High molecular weight kininogen or its light chain protects human plasma kallikrein from inactivation by plasma protease inhibitors,” *Biochemistry*, vol. 21, no. 3, pp. 567–572, Feb. 1982, doi: 10.1021/bi00532a024.

7. R. Zhuo, C. A. Siedlecki, and E. A. Vogler, “Autoactivation of blood factor XII at hydrophilic and hydrophobic surfaces,” *Biomaterials*, vol. 27, no. 24, pp. 4325–4332, Aug. 2006, doi: 10.1016/j.biomaterials.2006.04.001.

8. C. Puy *et al.*, “Factor XII promotes blood coagulation independent of factor XI in the presence of long chain polyphosphate,” *J Thromb Haemost*, vol. 11, no. 7, pp. 1341–1352, Jul. 2013, doi: 10.1111/jth.12295.

9. J. Bäck, J. Sanchez, G. Elgue, K. N. Ekdahl, and B. Nilsson, “Activated human platelets induce factor XIIa-mediated contact activation,” *Biochemical and Biophysical Research Communications*, vol. 391, no. 1, pp. 11–17, Jan. 2010, doi: 10.1016/j.bbrc.2009.10.123.

10. A. F. B. Omar and M. Z. B. MatJafri, “Turbidimeter Design and Analysis: A Review on Optical Fiber Sensors for the Measurement of Water Turbidity,”

Sensors (Basel), vol. 9, no. 10, pp. 8311–8335, Oct. 2009, doi: 10.3390/s91008311.

11. S. A. Smith and J. H. Morrissey, "Polyphosphate enhances fibrin clot structure," *Blood*, vol. 112, no. 7, pp. 2810–2816, Oct. 2008, doi: 10.1182/blood-2008-03-145755.

12. K. N. Sask, W. G. McClung, L. R. Berry, A. K. C. Chan, and J. L. Brash, "Immobilization of an antithrombin–heparin complex on gold: Anticoagulant properties and platelet interactions," *Acta Biomaterialia*, vol. 7, no. 5, pp. 2029–2034, May 2011, doi: 10.1016/j.actbio.2011.01.031.

13. K. G. Mann, M. F. Whelihan, S. Butenas, and T. Orfeo, "Citrate anticoagulation and the dynamics of thrombin generation," *Journal of Thrombosis and Haemostasis*, vol. 5, no. 10, pp. 2055–2061, 2007, doi: https://doi.org/10.1111/j.1538-7836.2007.02710.x.

14. E. R. Fischer, B. T. Hansen, V. Nair, F. H. Hoyt, and D. W. Dorward, "Scanning Electron Microscopy," *Current Protocols in Microbiology*, vol. 25, no. 1, p. 2B.2.1-2B.2.47, 2012, doi: 10.1002/9780471729259.mc02b02s25.

15. E. L. Hethershaw *et al.*, "The effect of blood coagulation factor XIII on fibrin clot structure and fibrinolysis," *Journal of Thrombosis and Haemostasis*, vol. 12, no. 2, pp. 197–205, 2014, doi: https://doi.org/10.1111/jth.12455.

16. J. W. Weisel and C. Nagaswami, "Computer modeling of fibrin polymerization kinetics correlated with electron microscope and turbidity observations: clot structure and assembly are kinetically controlled.," *Biophys J*, vol. 63, no. 1, pp. 111–128, Jul. 1992.

17. R. Khalifehzadeh, W. Ciridon, and B. D. Ratner, "Surface fluorination of polylactide as a path to improve platelet associated hemocompatibility," *Acta Biomaterialia*, vol. 78, pp. 23–35, Sep. 2018, doi: 10.1016/j.actbio.2018.07.042.

18. T. A. Horbett, "Fibrinogen adsorption to biomaterials," *J Biomed Mater Res A*, vol. 106, no. 10, pp. 2777–2788, Oct. 2018, doi: 10.1002/jbm.a.36460.

19. C. Sperling, M. Fischer, M. F. Maitz, and C. Werner, "Blood coagulation on biomaterials requires the combination of distinct activation processes," *Biomaterials*, vol. 30, no. 27, pp. 4447–4456, Sep. 2009, doi: 10.1016/j.biomaterials.2009.05.044.

20. O. J. T. McCarty *et al.*, “Rac1 Is Essential for Platelet Lamellipodia Formation and Aggregate Stability under Flow,” *J Biol Chem*, vol. 280, no. 47, pp. 39474–39484, Nov. 2005, doi: 10.1074/jbc.M504672200.

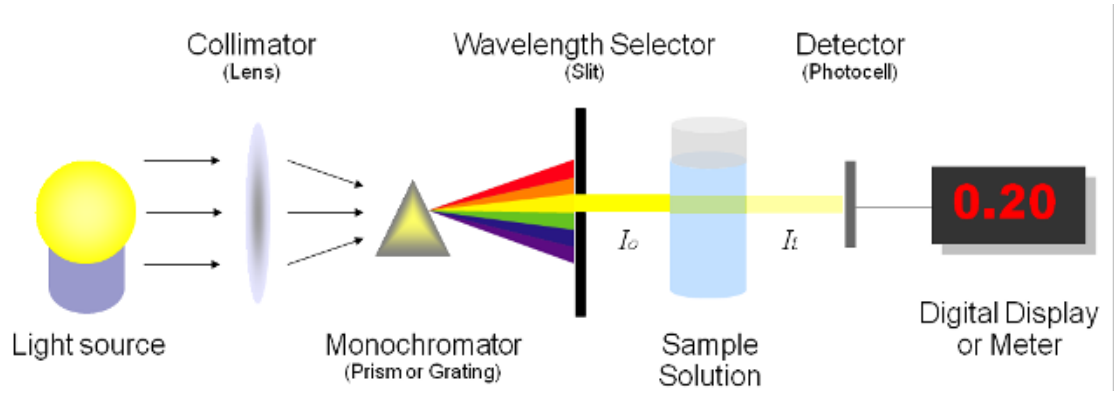

Figure 2.1. Schematic of spectrophotometer. Light is focused through a monochromator, a wavelength is selected, and the transmitted light intensity is measured.

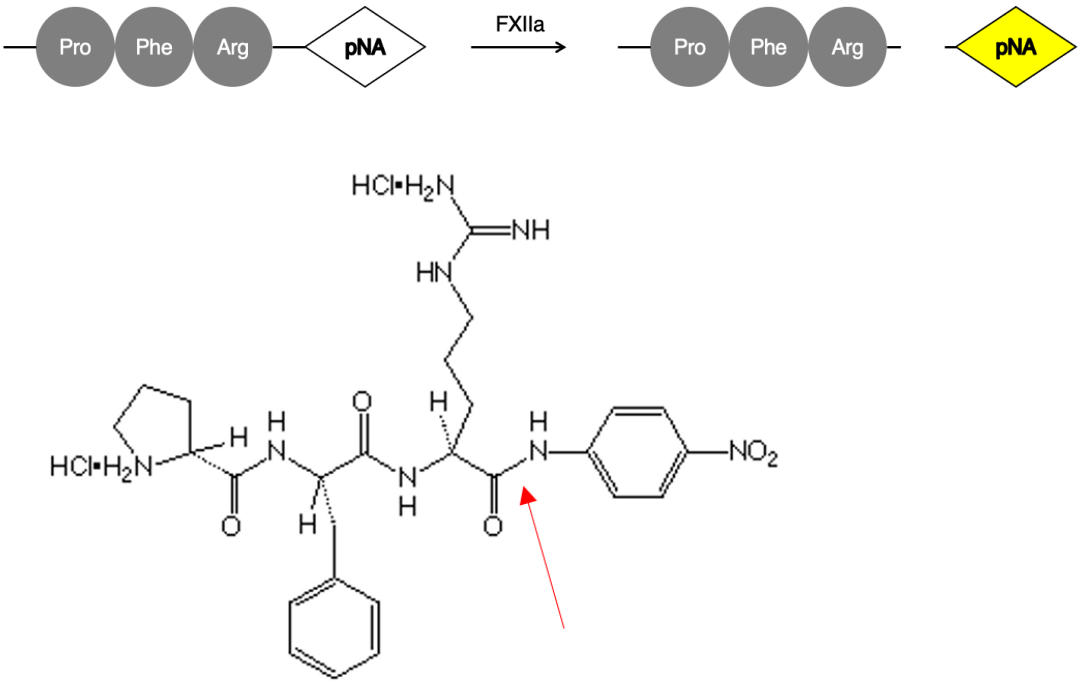

Figure 2.2. Schematic of FXIIa cleavage of bond on chromogenic substrate. Top. FXIIa cleaves paranitroaniline (pNA) from a signaling sequence of amino acids, resulting in pNA transitioning from colorless to yellow. Bottom. Molecular structure of chromogenic substrate with bond cleavage indicated (Chromogenix).

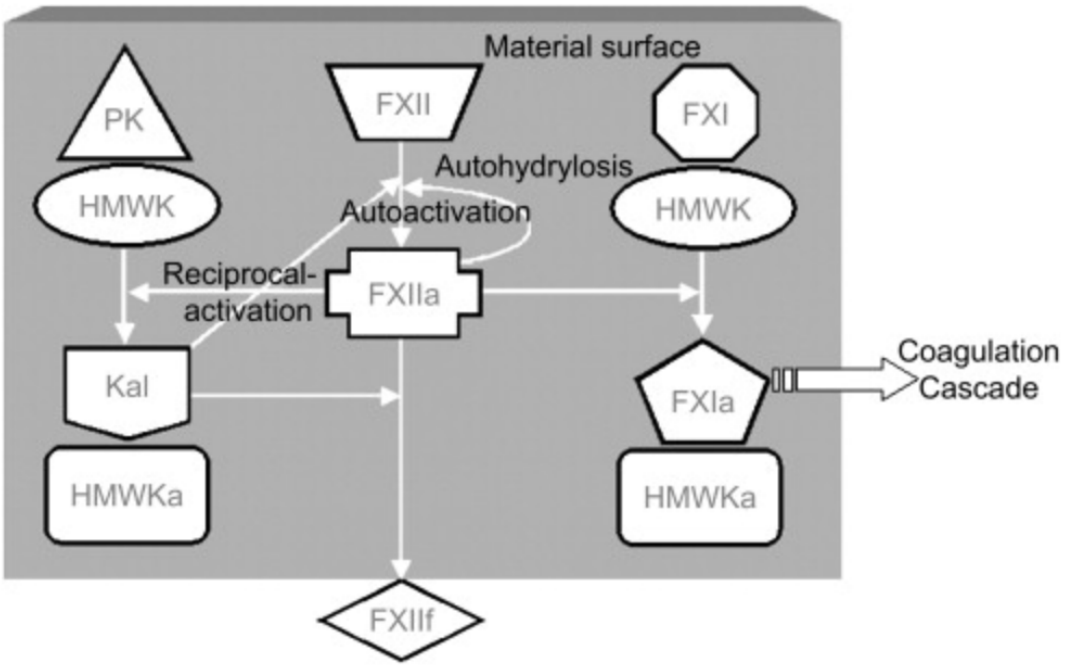

Figure 2.3. Mechanism of activation of FXII. Contact autoactivation occurs when FXII undergoes a conformational change when bound to a surface. Reciprocal activation occurs when FXII cleaves kallikrein from a complex of PK and HMWK. Autohydrolysis occurs when FXIIa hydrolyzes FXII into FXIIa (figure from Xu *et al.* 2014 [5]).

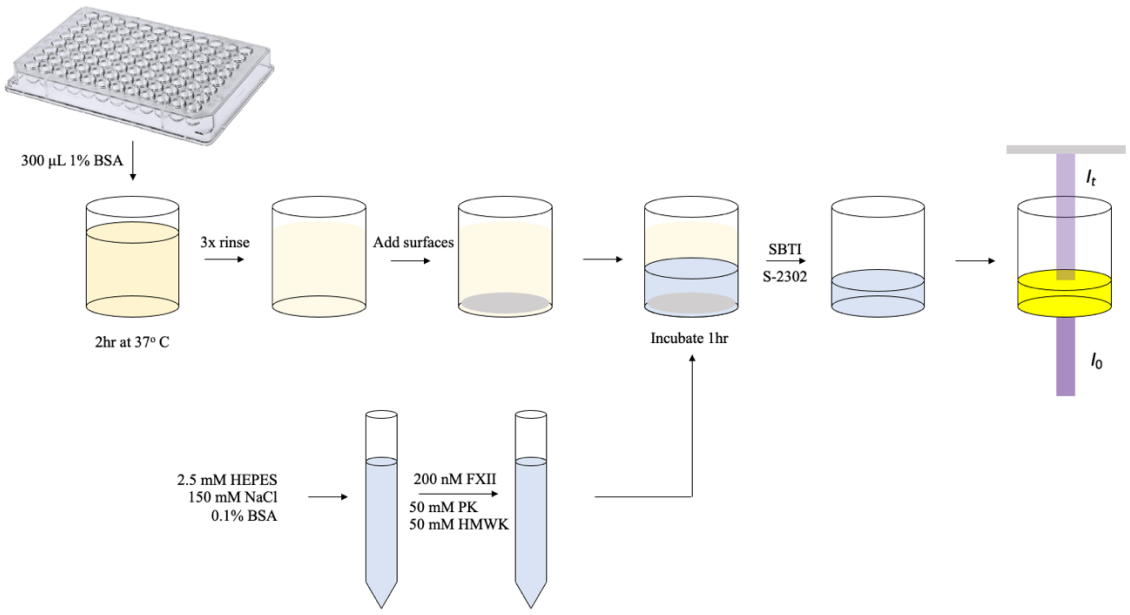

Figure 2.4**.** Schematic of FXIIa assay procedure. Wells of a 96-well plate are blocked with BSA. Surfaces and FXII (with or without cofactors PK and HMWK) in buffer is added to wells. FXII solution is incubated on surfaces in wells, transferred to a new plate, and quenched with soybean trypsin inhibitor. A chromogenic substrate is added and the absorbance is measured over time.

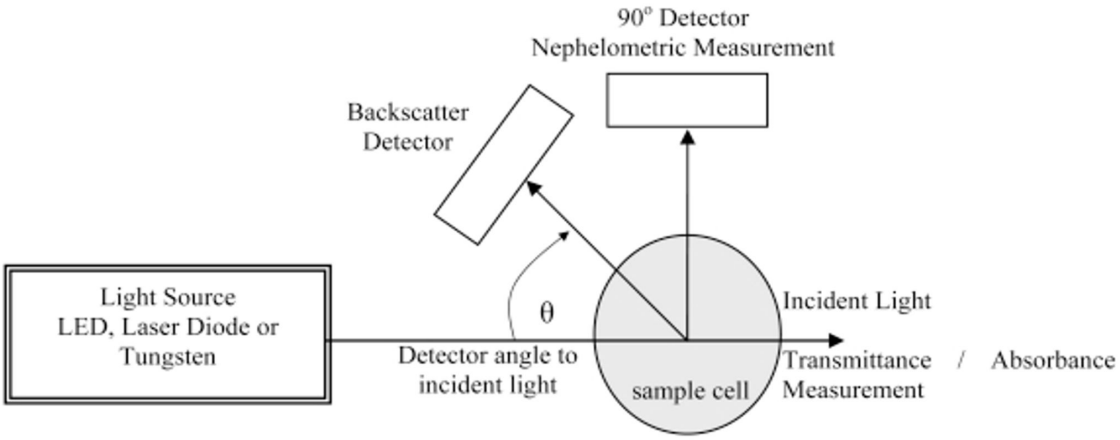

Figure 2.5**.** Schematic of turbidimeter. Light is focused through a sample and the transmitted light intensity and backscattered photons are measured (Figure from Omar *et al.* 2009 [10]).

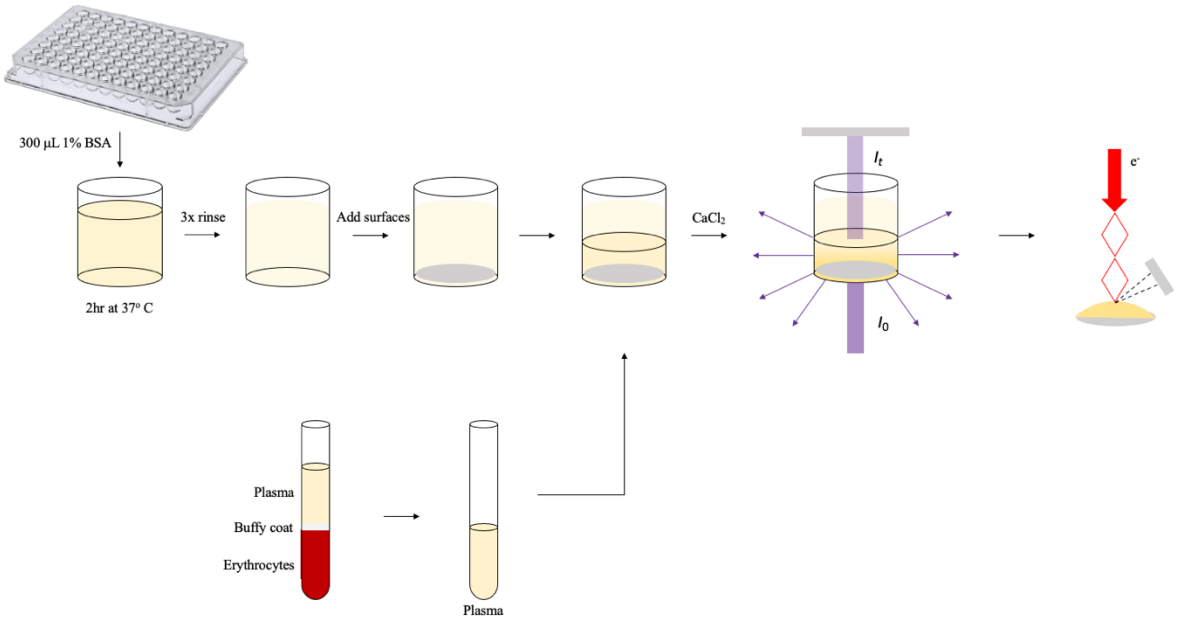

Figure 2.6. Schematic of fibrin generation procedure. Wells of a 96-well plate are blocked with BSA. Surfaces, buffer, and platelet-poor plasma are added to wells. The plasma is recalcified and the absorbance is measured over time. The clots are then prepared for SEM and imaged.

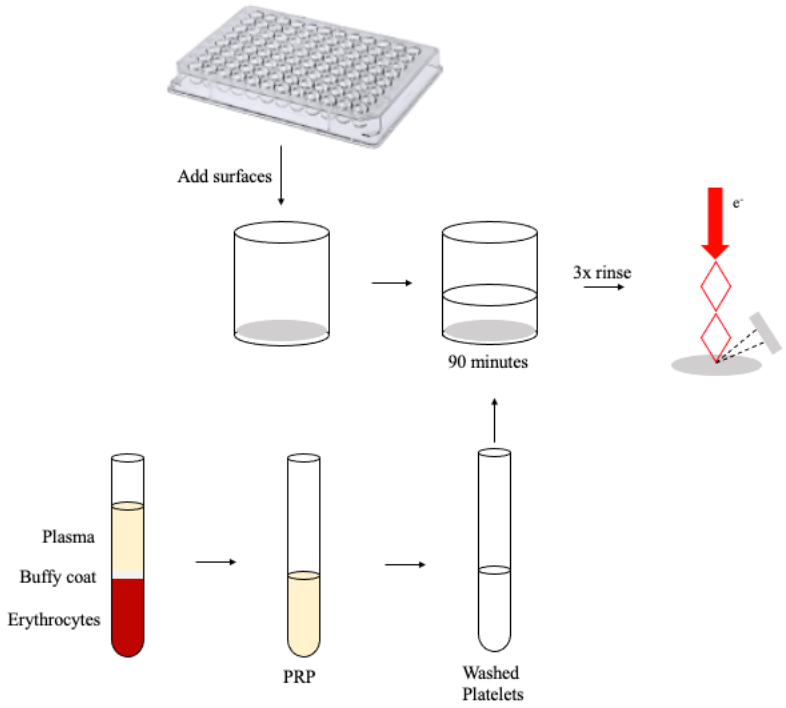

Figure 2.7. Schematic of platelet adhesion procedure. To prepare samples, platelets in neat buffer are incubated on a surface. The surface is then rinsed to remove all non-adherent material, then fixed, dehydrated, and sputter coated to prepare for imaging.

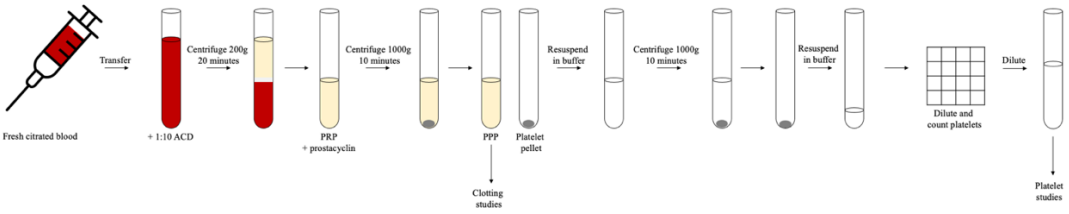

Figure 2.8. Schematic of blood processing procedure. Plasma is isolated from erythrocytes and leukocytes, then platelets are isolated from plasma by centrifugation. Resultant platelet-poor plasma is used for fibrin generation studies. Resultant platelet pellet is reconstituted in buffer and used for platelet studies.

Chapter 3 – Hemocompatibility Analysis of Bioinspired Coating for Photoreactor

Madeleine H. Hummel, Ryan A. Faase, Joe E. Baio
School of Chemical, Biological, and Environmental Engineering Oregon State University, OR, USA

Abstract

Surface-associated thrombosis is a critical concern in medical device development. Current extracorporeal circulation units require systemic anticoagulation to avoid thrombosis, which can cause adverse effects such as thrombocytopenia, hypertriglyceridemia, and hyperkalemia. To address this issue, we combine the technology of polydopamine (PDA) functionalization with slippery liquid infused porous surfaces (SLIPS). PDA readily coats a wide variety of surfaces and can be functionalized via Michael Addition. We functionalized PDA with a thiolated fluoropolymer to form a pseudo self-assembled monolayer (pSAM) that serves as the porous surface component of SLIPS, then added liquid perfluorodecalin to complete the SLIPS coating. We hypothesized that the PDA SLIPS coating provides enhanced hemocompatibility due to its omniphobic properties and composition of compounds currently used in medical applications. The coatings were evaluated for thrombogenicity via quantification of Factor XII (FXII) activation, fibrin formation, and platelet adhesion. The SLIPS coating activated 50% less FXII than glass and 100% more FXII than bovine serum albumin (BSA) coated substrates. SLIPS had similar plasma clotting time to BSA and plasma clotted two times slower on SLIPS than on glass. Platelet adhesion was increased two-fold on SLIPS compared to BSA and decreased two-fold on SLIPS compared to glass.

3.1 Introduction

Phototherapy treatment of hyperbilirubinemia in newborns requires the exposure of blue light to convert neurotoxic bilirubin to excretable lumirubin in the blood [1, 2]. To treat more severe cases of hyperbilirubinemia, the blood can be directly exposed to blue LEDs via an extracorporeal circulation unit equipped with a photoreactor. Previous work has shown the efficacy of photoreactor treatment in a Gunn rat model, though systemic anticoagulation was required. To prevent thrombus formation while avoiding systemic anticoagulation, the photoreactor must be modified with an antithrombogenic coating.

Hemocompatible coatings for extracorporeal circulation units - and more broadly, blood-contacting medical devices - is a clinical need that remains unsolved despite many proposed solutions. There are three approaches of surface modification to control thrombus formation: surface passivation, surface activation, and biomimicry [3]. Surface passivation is the engineering of a material such that interactions between the material surface and blood are limited. Common examples of surface passivation are binding zwitterionic polymers to material surfaces and inclusion of hydrophilic polymers at the material surface [4, 5]. Surface activation involves binding bioactive molecules to the surface to actively combat coagulation. Heparin is a commonly used clinical systemic anticoagulant that works by binding and activating antithrombin, which in turn inactivates thrombin and prevents thrombus formation [6, 7]. Surface-bound heparin is an example of surface activation, as heparin actively works to prevent thrombin formation. Biomimicry for blood compatibility is the engineering of a surface to mimic the microenvironment of a native blood vessel. This includes porous materials to promote tissue ingrowth and other tissue engineering applications [8].

Slippery liquid infused porous surfaces (SLIPS) represent a novel method of surface passivation that involves trapping a liquid, often an oil, onto a porous surface [9, 10].

The result is an antifouling surface that has been proposed to resist adhesion of coagulation factors [9, 10]. Testing of coagulation factor activation, specifically FXII, and plasma clotting kinetics on SLIPS surfaces has not been previously studied.

Previous SLIPS coatings used plasma treatment to graft polymers to the surface. The drawback of this method is the requirement for specialized equipment and infrastructure to manufacture the coating. To increase ease of manufacturing, polydopamine (PDA) can be coated onto the substrate and a thiolated fluoropolymer can be attached via Michael addition [11, 12] (Figure 3.1). PDA and SLIPS coatings have been proposed to be anti-fouling and hemocompatible, though limited testing on specific coagulation activity of SLIPS has been done [10, 13, 14]. Experimental surfaces were the bare substrate (cyclic olefin copolymer - COC), PDA-coated COC (PDA), pSAM surfaces (PDA-FDT), and the pSAM SLIPS surface (PDA-FDT-PFD). To biologically characterize the PDA SLIPS coating, we tested the resistance of the coating to FXII activation, clot formation, clot stability, and platelet adhesion. FXII activation gives insight into the extent of intrinsic coagulation. On biocompatible surfaces, we would expect to see a lower concentration of activated FXII (FXIIa) than on prothrombogenic surfaces. Platelet adhesion and activation testing describes the tendency of platelets to adhere to a surface, which promotes coagulation. We would expect to see fewer adherent platelets on biocompatible surfaces compared to prothrombogenic surfaces. Fibrin generation time describes the resistance to fibrin formation from fibrinogen, and thus clot formation. Biocompatible coatings will have a longer fibrin generation time than prothrombogenic coatings. Clot stability, quantified via crosslinking density measurements, provides insight into the ability of a clot to break down. Clots on biocompatible coatings should be less stable (larger fiber diameter and lower crosslinking density) compared to prothrombogenic surfaces. Together these assays provide a starting point for understanding the behavior of PDA SLIPS when in contact with blood. We expect the PDA SLIPS coating to exhibit antithrombogenic properties, therefore we expect a lower

concentration of FXII, decreased platelet adhesion, longer fibrin generation time, and lower clot stability compared to other surfaces.

3.2 Materials and Methods

3.2.1 Surface Preparation

The substrate used for this study was cyclic olefin copolymer (COC). COC was cut into 5mm diameter coupons were cut using a Universal laser cutter. The substrates were cleaned by sonication in a solution of 50% ethanol and 50% acetone by volume for 10 minutes, rinsing with ethanol, then sonication in MilliQ water for 10 minutes, and rinsing in MilliQ water. Coupons were dried and stored in nitrogen until ready for use.

Samples were prepared as described previously [15]. Briefly, dopamine was polymerized on substrate surfaces by incubating in 2mg/mL dopamine and 10mM Tris for 24 hours. Next, surfaces were incubated in 10mM fluorinated dodecanethiol (FDT) and 10mM triethylamine (TEA) for 24 hours. Samples were rinsed and stored in nitrogen until ready to use. Immediately prior to use, a layer of liquid perfluorodecalin (PFD) was added to the surface (Figure 3.1).

BSA was used as a negative control. BSA-coated surfaces were prepared by incubating surfaces in 1% BSA in MilliQ water for 2 hours at 37^{o} C. Glass was used as a positive control and cleaned with ethanol prior to use. Experimental surfaces were the bare substrate (COC), PDA-coated COC (PDA), pSAM surfaces (PDA-FDT), and the pSAM SLIPS surface (PDA-FDT-PFD).

3.2.2. Contact Angle

Surfaces were characterized as described previously [15]. Contact angle measurements were performed prior to hemocompatibility experiments to confirm

surfaces have been modified. The contact angle of at least two drops on each surface were measured prior to hemocompatibility studies.

A laboratory contact angle setup was constructed based on the method of Lamour et. al [16]. Briefly, a stage, lens, and smartphone holder were mounted to a breadboard. A lamp was used as a light source behind the stage. Contact angle measurements were taken using ImageJ by approximating the surface as a line and the water droplet as an ellipse.

3.2.3 Platelet-Poor Plasma and Washed Platelet Preparation

Human blood samples were collected from volunteers at Oregon State University Student Health Services in accordance with an approved IRB. Blood samples were processed following the method of McCarty *et al.* [17]. Approximately 15mL of blood was drawn into sodium citrate Vacutainers. Acid-citrate-dextrose (ACD) was added to the whole blood at a 1:10 volume ratio. Blood was centrifuged at 200g for 20 minutes at room temperature. The supernatant platelet-rich plasma was transferred and 0.1ug/mL prostaglandin I2 was added to inhibit platelet activation. Platelet-rich plasma was centrifuged at 1000g for 10 minutes at room temperature. The supernatant platelet-poor plasma was transferred and used for fibrin generation studies. The platelet pellet was resuspended in Tyrode's buffer (129mM NaCl, 20mM HEPES, 12mM NaHCO3, 2.9mM KCl, 1mM MgCl2, 0.34mM Na2HPO4) and 0.1µg/mL prostaglandin I2 was added. The platelets were centrifuged at 1000g for 10 minutes, the supernatant was discarded, and pelleted platelets were resuspended in Tyrode's buffer. Platelets were counted using a hemocytometer and the platelet solution was diluted to a concentration of $1x10^8$ platelets/mL [18, 19].

3.2.4 FXIIa Assay

Wells of interest of a nontreated 96-well polystyrene were blocked with 300µL 1% BSA in MilliQ water for 2 hours at 37° C. After 2 hours, wells were rinsed 3x with

MilliQ water. Plates were coated immediately prior to use. FXIIa assays were performed using methods adapted from Bates *et al.* [18]. A solution of FXII (200nM), PK (50nM), and HMWK (50nM) in vacuum filtered and degassed buffer (25mM HEPES pH 7.4, 150mM NaCl, and 0.1% BSA) was prepared and 120µL was added to each well of a 96-well plate blocked with BSA. After incubation for 60 minutes, 90µL of protein solution was removed and added to a new plate containing 5µL 4.7mM soybean trypsin inhibitor (Sigma). 5µL of chromogenic substrate S-2302 (Chromogenix) was added to each well and the absorbance was measured at 405nm every 1 minute for 60 minutes using a FlexStation 3 microplate reader (Molecular Devices). A standard curve was used to determine the concentration of FXIIa from the measured OD. A BSA-blocked well was used as a negative control and glass was used as a positive control. Three separate experiments were performed for a total sample size of 18.

3.2.5 Clot Turbidity Analysis

Wells of interest of a non-treated polystyrene 96-well plate were blocked with 300µL 1% BSA in MilliQ water for 2 hours at 37°C. After 2 hours, wells were rinsed 3x with MilliQ water. Plates were coated immediately prior to use. Fibrin generation experiments were performed on a FlexStation 3 (Molecular Devices) using methods adapted from Bates et al. and Sask *et al*. [18, 20]. 50µL of platelet poor plasma (PPP) from fresh human blood samples from two donors was added to wells with or without surfaces, along with 50uL buffer (25mM HEPES pH 7.4, 150mM NaCl). Plasma was then recalcified with 50uL 25mM $CaCl_2$. Absorbance measurements were taken every 1 minute for 60 minutes at 405nm. Three separate experiments were performed for a total sample size of 18 per donor.

Fibrin generation time was defined as the time to reach a 5% increase over the baseline absorbance value. 5% is a sufficient threshold to overcome the noise floor of the data [18].

3.2.6 Clot Morphology

Wells of interest of a non-treated 96-well polystyrene were blocked with 300µL 1% BSA in MilliQ water for 2 hours at 37° C. After 2 hours, wells were rinsed 3x with MilliQ water. Plates were coated immediately prior to use. Clots were prepared using the same method as turbidity analysis, but clots were allowed to form for 5x the fibrin generation time to ensure samples were fully clotted. Fibrin clots and surfaces were removed from wells and fixed in 1% paraformaldehyde and 2.5% glutaraldehyde in 0.1M sodium cacodylate buffer overnight. Samples were then rinsed twice in 0.1M cacodylate buffer for 15 minutes each. Samples were dehydrated in a graded series of ethanol (10%, 30%, 50%, 70%, 90%, 95%, 100%) for 10-15 minutes each, followed by critical point drying (Electron Microscopy Sciences). Samples were sputter coated with gold/palladium (Cressington 108A) and imaged on an SEM (FEI Quanta 600F).

ImageJ was used to measure fiber diameter and clot density. Clot density was determined by drawing a line through the image and counting the number of times a fiber crosses the line [21]. The diameter of 10 fibers was per spot per sample were measured. 3 lines of 4µm in length were drawn per spot per sample. Two samples per sample group were analyzed and the experiment was repeated twice.

3.2.7 Platelet Adhesion and Activation

10^8 platelets/mL in Tyrode's buffer were incubated on surfaces in a 96-well plate for 2 hours at 37° C. Surfaces were rinsed with Tyrode's buffer five times to remove non-adherent and loosely bound platelets. The samples were then fixed and prepared for SEM using the same method as for the clots. At least three spots per sample and two samples per sample group were imaged. Two donors were used and the experiment was repeated twice.

ImageJ was used to count the number of adherent platelets and calculate average cell area. The average cell area describes where on average platelets fall on the spectrum of activation. Inactive discoid platelets have a smaller area than active spread platelets, at approximately 2-10 μm^2 and 20-50 μm^2, respectively.

3.2.8 Statistical analysis

All statistical analysis was performed using JMP. For data that was normalized to glass, the error from glass is imbedded in the reported standard deviation. For each test, a one-way ANOVA and a Tukey post-hoc comparison were performed to determine differences between means.

3.3 Results

FXIIa concentration, fibrin generation time, clot morphology, and platelet adhesion and activation were measured on PDA SLIPS surfaces.

3.3.1 Contact Angle

Water contact angle measurements were used to confirm each step of our surface modification process. Bare COC is hydrophobic, therefore as we modified the substrate with PDA we expected to observe a decrease in the observed water contact angle. Then when the thiol was added, the surface was expected to return to a hydrophobic state (Figure 3.1). Our clean COC substrate had an average contact angle of 85.2 degrees. After addition of the PDA, the surface became hydrophilic with a contact angle of 46.0 degrees. When the thiol was added, the surface became highly hydrophobic with a contact angle of 121.8 degrees (Figure 3.2). Two measurements were taken per sample prior to hemocompatibility assays and compared to established contact angle measurements [15].

3.3.2 FXIIa Assay

FXIIa concentration was determined at each step of our surface modification process. We expect to see less activation of FXII on PDA SLIPS surfaces compared to glass because glass is negatively charged. PDA SLIPS should have a lower concentration of FXIIa compared to PDA and COC because we hypothesize that the surface is omniphobic, resisting protein adhesion. FXII did not autoactivate in neat buffer on all PDA SLIPS surfaces and did autoactivate on glass surfaces. When PK and HMWK were present in solution, FXII activation was observed on all samples. FXII activation on PDA was not statistically significantly different from glass. COC, PDA-FDT and PDA-FDT-PFD activated 50% less FXII than PDA and glass, but 100% more than BSA (Figure 3.3).

3.3.3 Clot Turbidity Analysis

Fibrin generation time was determined on BSA, glass, bare COC, and PDA-FDT-PFD. We expected to observe a longer fibrin generation time on PDA-FDT-PFD than glass and COC because of the hypothesized antithrombogenic behavior due to omniphobicity of SLIPS. Platelet poor plasma (PPP) clotted approximately 2.5x slower on PDA-FDT-PFD than glass for all runs and there was no difference between PDA-FDT-PFD and BSA or COC (Figure 3.4). There was significant variation between donors and between runs, but the trends remained consistent. Differences between runs were not of interest, so data was normalized to glass fibrin generation time. Samples were isolated from 3 distinct draws from each of two donors for a total sample size of 14 per sample per donor.

3.3.4 Clot Morphology

Fiber diameter and crosslinking density measurements were taken from SEM micrographs. Less stable clots exhibit larger fiber diameter and more porous fibrin networks. PDA-FDT-PFD was expected to have larger fiber diameter and a less crosslinked network compared to glass and COC. Data was normalized to glass, and

PDA-FDT-PFD had approximately 20% higher fiber diameter and 25% lower clot density than glass (Figure 3.5). PDA-FDT-PFD also had significantly higher fiber diameter and lower clot density than BSA and COC, suggesting that clots formed on PDA-FDT-PFD are less stable and easier to break down than clots formed on glass, COC and BSA [21]. Representative SEM micrographs are shown in Figure 3.6.

3.3.5 Platelet Adhesion and Activation

Platelet adhesion was quantified from SEM micrographs. SLIPS surfaces have been shown to resist platelet adhesion due to their omniphobic properties [10, 22]. We expected to see no or minimal adherent platelets on PDA-FDT-PFD surfaces. Purified platelets were incubated with surfaces for 90 minutes, then triple rinsed, fixed and dehydrated in preparation for imaging. The HFW was set to 64μm and the surface area for analysis was 3520 μm^2 (Figure 3.7) and data was normalized to glass. There was approximately 150% lower adhesion to BSA coated surfaces than all other groups. There was no difference in platelet adhesion between PDA-FDT-PFD, COC and glass for donor A1 and glass had significantly higher platelet adhesion than PDA-FDT-PFD and COC for donor A3. (Figure 3.8).

3.4 Discussion

SLIPS coatings are a promising development in anti-fouling and anti-thrombogenic surface modification due to their potential omniphobic properties. The combination of SLIPS technology with the ability to universally coat any substrate with PDA, provides a platform for easily manufactured SLIPS coatings. Despite their promise, the specific interactions between SLIPS coatings and blood, however, remains poorly understood. Here, in this investigation PDA SLIPS coatings were characterized in terms of FXII activation, fibrin generation time, clot morphology, and platelet adhesion and activation.

As mentioned earlier, quantification of the activation of intrinsic coagulation on SLIPS surfaces has not been investigated previously. Badv *et al*. hypothesized in 2017 that the prolonged clotting time they observed on SLIPS-coated catheter sheathing was due to reduced activation of the contact system, which would suggest a lower concentration of FXIIa on their surfaces [13]. Previously, it has been shown that FXII activation is reduced at hydrophilic surfaces [23]. potentially due to trapping of a liquid layer causing reduced protein adhesion. While activation is decreased on hydrophilic surfaces, it is elevated on negatively charged surfaces like glass [24]. In this work, we used BSA coated surfaces as a negative control and glass as a positive control. A 3x increase in FXII activation on bare glass compared to BSA was reported previously, which is consistent with our results [18]. We observed a ~65% increase in FXII activation on PDA-FDT-PFD compared to BSA and a ~40% reduction in FXII activation on PDA-FDT-PFD compared to glass. This suggests that there is FXII coming down onto the surface of our coating and activating, though to a lesser degree than glass. However, we observed no difference in FXII activation between PDA and glass, which is unsurprising given that both surfaces are hydrophilic. There was also no observed difference in FXII activation between COC and PDA-FDT-PFD, suggesting COC exhibits similar intrinsic coagulation behavior to PDA-FDT-PFD.

Next, we tracked the fibrin generation kinetics of platelet poor plasma across all our experimental and control surfaces. Our observed range of fibrin generation time of approximately 5-30 minutes were consistent with those reported in literature using similar methods of turbidimetric quantification on other experimental surfaces [18, 25]. We observed that plasma clotted 2.5x slower on PDA-FDT-PFD than glass and there was no significant difference between PDA-FDT-PFD, BSA or COC. The observed differences in FXII activation between BSA and PDA-FDT-PFD, combined with the lack of observed differences in plasma clotting time, would suggest that

PDA-FDT-PFD induces an antithrombogenic pathway that is different than the typical intrinsic coagulation behavior.

Previously, SLIPS coatings were observed to resist platelet adhesion in whole blood and platelet rich plasma adhesion assays [10, 22]. However, no work has been done previously in a purified platelet system which allow for identifying the specific interactions between platelets and surfaces independent of protein adsorption or other events that may take place within whole blood and plasma studies. In our purified platelet system, we observed a 150% increase in adherent platelets on PDA-FDT-PFD compared to BSA and a 50% decrease in adherent platelets on PDA-FDT-PFD compared to glass. This suggests that the SLIPS coating is not omniphobic as adherent cells are observed.

This work demonstrates that this formulation of a SLIPS coating is not omniphobic as FXII activated on the surface and platelets adhered to the coating. The observed prolonged fibrin generation time in PPP, however, suggests that SLIPS could still exhibit antithrombogenic behavior. The FXII assay and platelet adhesion studies were performed in a purified system to gather information on isolated surface interactions, whereas the fibrin generation study was performed using PPP to investigate comprehensive hematologic behavior of the surfaces. This suggests that the SLIPS coating could have a high affinity for a passivating blood protein or low affinity for an active procoagulant. More work on specific coagulation factor adsorption and activation, such as thrombin, fibrinogen, and complement system proteins is needed to fully characterize the surface. Studies on FXII and platelet adhesion in plasma and whole blood models would provide more insight into observed activation in a purified system.

3.5 Conclusion

This work suggests that PDA SLIPS coatings prevent plasma clotting, but FXII activates on the surface and adherent and activated platelets were observed. A limitation of this study is that FXII activation and platelet adhesion were not normalized for protein adhesion. Another limitation was the absence of flow. Future work will involve the comparison of purified FXII and platelet assays to plasma and whole blood models and incorporate physiological flow conditions to investigate blood interactions under shear. This work provides insight into how SLIPS may be utilized and further characterized for blood-contacting medical device applications.

3.6 References

1. N. Capková *et al.*, "The Effects of Bilirubin and Lumirubin on the Differentiation of Human Pluripotent Cell-Derived Neural Stem Cells," *Antioxidants (Basel)*, vol. 10, no. 10, p. 1532, Sep. 2021, doi: 10.3390/antiox10101532.

2. J. Wang, G. Guo, A. Li, W.-Q. Cai, and X. Wang, "Challenges of phototherapy for neonatal hyperbilirubinemia (Review)," *Experimental and Therapeutic Medicine*, vol. 21, no. 3, pp. 1–1, Mar. 2021, doi: 10.3892/etm.2021.9662.

3. X. Liu *et al.*, "Blood compatible materials: state of the art," *J. Mater. Chem. B*, vol. 2, no. 35, pp. 5718–5738, Aug. 2014, doi: 10.1039/C4TB00881B.

4. P.-S. Liu *et al.*, "Grafting of Zwitterion from Cellulose Membranes via ATRP for Improving Blood Compatibility," *Biomacromolecules*, vol. 10, no. 10, pp. 2809–2816, Oct. 2009, doi: 10.1021/bm9006503.

5. Y. Chang, W.-J. Chang, Y.-J. Shih, T.-C. Wei, and G.-H. Hsiue, "Zwitterionic Sulfobetaine-Grafted Poly(vinylidene fluoride) Membrane with Highly Effective Blood Compatibility via Atmospheric Plasma-Induced Surface Copolymerization," *ACS Appl. Mater. Interfaces*, vol. 3, no. 4, pp. 1228–1237, Apr. 2011, doi: 10.1021/am200055k.

6. R. Carrell, R. Skinner, M. Wardell, and J. Whisstock, "Antithrombin and heparin," *Molecular Medicine Today*, vol. 1, no. 5, pp. 226–231, Aug. 1995, doi: 10.1016/S1357-4310(95)91494-3.

7. L. Jin, J. P. Abrahams, R. Skinner, M. Petitou, R. N. Pike, and R. W. Carrell, "The anticoagulant activation of antithrombin by heparin," *Proc Natl Acad Sci U S A*, vol. 94, no. 26, pp. 14683–14688, Dec. 1997.

8. L. Bordenave, M. Rémy-Zolghadri, P. Fernandez, R. Bareille, and D. Midy, "Clinical performance of vascular grafts lined with endothelial cells," *Endothelium*, vol. 6, no. 4, pp. 267–275, 1999, doi: 10.3109/10623329909078494.

9. T.-S. Wong *et al.*, "Bioinspired self-repairing slippery surfaces with pressure-stable omniphobicity," *Nature*, vol. 477, no. 7365, Art. no. 7365, Sep. 2011, doi: 10.1038/nature10447.

10. D. C. Leslie *et al.*, “A bioinspired omniphobic surface coating on medical devices prevents thrombosis and biofouling,” *Nature Biotechnology*, vol. 32, no. 11, Art. no. 11, Nov. 2014, doi: 10.1038/nbt.3020.

11. C.-Y. Liu and C.-J. Huang, “Functionalization of Polydopamine via the Aza-Michael Reaction for Antimicrobial Interfaces,” *Langmuir*, vol. 32, no. 19, pp. 5019–5028, May 2016, doi: 10.1021/acs.langmuir.6b00990.

12. L.-C. Xu, J. W. Bauer, and C. A. Siedlecki, “Proteins, platelets, and blood coagulation at biomaterial interfaces,” *Colloids and Surfaces B: Biointerfaces*, vol. 124, pp. 49–68, Dec. 2014, doi: 10.1016/j.colsurfb.2014.09.040.

13. M. Badv, I. H. Jaffer, J. I. Weitz, and T. F. Didar, “An omniphobic lubricant-infused coating produced by chemical vapor deposition of hydrophobic organosilanes attenuates clotting on catheter surfaces,” *Scientific Reports (Nature Publisher Group)*, vol. 7, pp. 1–10, Sep. 2017, doi: http://dx.doi.org.ezproxy.proxy.library.oregonstate.edu/10.1038/s41598-017-12149-1.

14. K. Manabe, K.-H. Kyung, and S. Shiratori, “Biocompatible Slippery Fluid-Infused Films Composed of Chitosan and Alginate via Layer-by-Layer Self-Assembly and Their Antithrombogenicity,” *ACS Appl. Mater. Interfaces*, vol. 7, no. 8, pp. 4763–4771, Mar. 2015, doi: 10.1021/am508393n.

15. R. A. Faase, “Spherical Au Nanoparticle Interaction with Lipid Monolayers Probed with Sum Frequency Generation Spectroscopy.”

16. G. Lamour *et al.*, “Contact Angle Measurements Using a Simplified Experimental Setup,” *J. Chem. Educ.*, vol. 87, no. 12, pp. 1403–1407, Dec. 2010, doi: 10.1021/ed100468u.

17. O. J. T. McCarty *et al.*, “Rac1 Is Essential for Platelet Lamellipodia Formation and Aggregate Stability under Flow,” *J Biol Chem*, vol. 280, no. 47, pp. 39474–39484, Nov. 2005, doi: 10.1074/jbc.M504672200.

18. N. M. Bates, C. Puy, P. L. Jurney, O. J. T. McCarty, and M. T. Hinds, “Evaluation of the Effect of Crosslinking Method of Poly(Vinyl Alcohol) Hydrogels on Thrombogenicity,” *Cardiovasc Eng Tech*, vol. 11, no. 4, pp. 448–455, Aug. 2020, doi: 10.1007/s13239-020-00474-y.

19. R. Khalifehzadeh, W. Ciridon, and B. D. Ratner, “Surface fluorination of polylactide as a path to improve platelet associated hemocompatibility,” *Acta*

Biomaterialia, vol. 78, pp. 23–35, Sep. 2018, doi: 10.1016/j.actbio.2018.07.042.

20. K. N. Sask, W. G. McClung, L. R. Berry, A. K. C. Chan, and J. L. Brash, "Immobilization of an antithrombin–heparin complex on gold: Anticoagulant properties and platelet interactions," *Acta Biomaterialia*, vol. 7, no. 5, pp. 2029–2034, May 2011, doi: 10.1016/j.actbio.2011.01.031.

21. E. L. Hethershaw *et al.*, "The effect of blood coagulation factor XIII on fibrin clot structure and fibrinolysis," *Journal of Thrombosis and Haemostasis*, vol. 12, no. 2, pp. 197–205, 2014, doi: https://doi.org/10.1111/jth.12455.

22. S. Yuan, S. Luan, S. Yan, H. Shi, and J. Yin, "Facile Fabrication of Lubricant-Infused Wrinkling Surface for Preventing Thrombus Formation and Infection," *ACS Appl. Mater. Interfaces*, vol. 7, no. 34, pp. 19466–19473, Sep. 2015, doi: 10.1021/acsami.5b05865.

23. R. Zhuo, C. A. Siedlecki, and E. A. Vogler, "Autoactivation of blood factor XII at hydrophilic and hydrophobic surfaces," *Biomaterials*, vol. 27, no. 24, pp. 4325–4332, Aug. 2006, doi: 10.1016/j.biomaterials.2006.04.001.

24. E. Stavrou and A. H. Schmaier, "Factor XII: What Does It Contribute To Our Understanding Of The Physiology and Pathophysiology of Hemostasis & Thrombosis," *Thromb Res*, vol. 125, no. 3, pp. 210–215, Mar. 2010, doi: 10.1016/j.thromres.2009.11.028.

25. K. N. J. Stevens, Y. B. J. Aldenhoff, F. H. van der Veen, J. G. Maessen, and L. H. Koole, "Bioengineering of Improved Biomaterials Coatings for Extracorporeal Circulation Requires Extended Observation of Blood-Biomaterial Interaction under Flow," *J Biomed Biotechnol*, vol. 2007, 2007, doi: 10.1155/2007/29464.

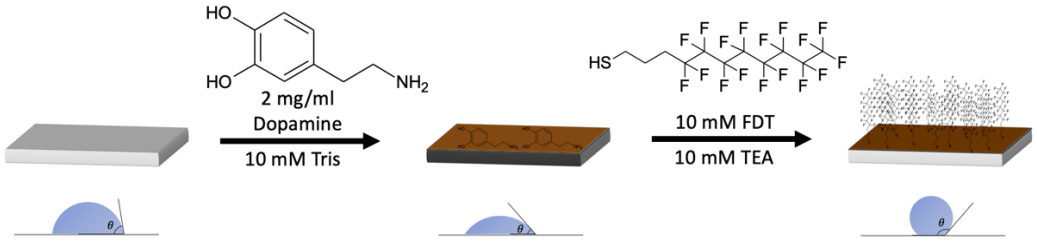

Figure 3.1. Schematic of PDA-FDT-PFD coating process. The bare substrate, COC (left) is hydrophobic. A layer of polydopamine (PDA) was added to the surface by incubating surfaces overnight with dopamine and Tris. PDA is hydrophilic, so the PDA coating step can be verified with water contact angle. Fluorinated dodecanethiol (FDT) was conjugated to the PDA surface by incubating overnight. FDT is hydrophobic, so this step can be verified with water contact angle measurements. Not pictured is the addition of perfluorodecalin (PFD) to the surface immediately prior to use.

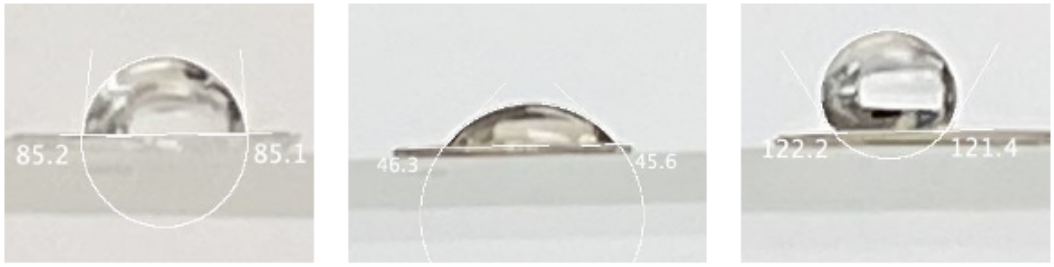

Figure 3.2. Water contact angle images of surfaces at each step of modification. Water contact angle was used to verify each step of the coating process on coupons prior to hemocompatibility analysis. The clean COC substrate is hydrophobic (left). After addition of the PDA layer, the surface becomes hydrophilic (middle). When the FDT layer is added the surface becomes hydrophobic (right).

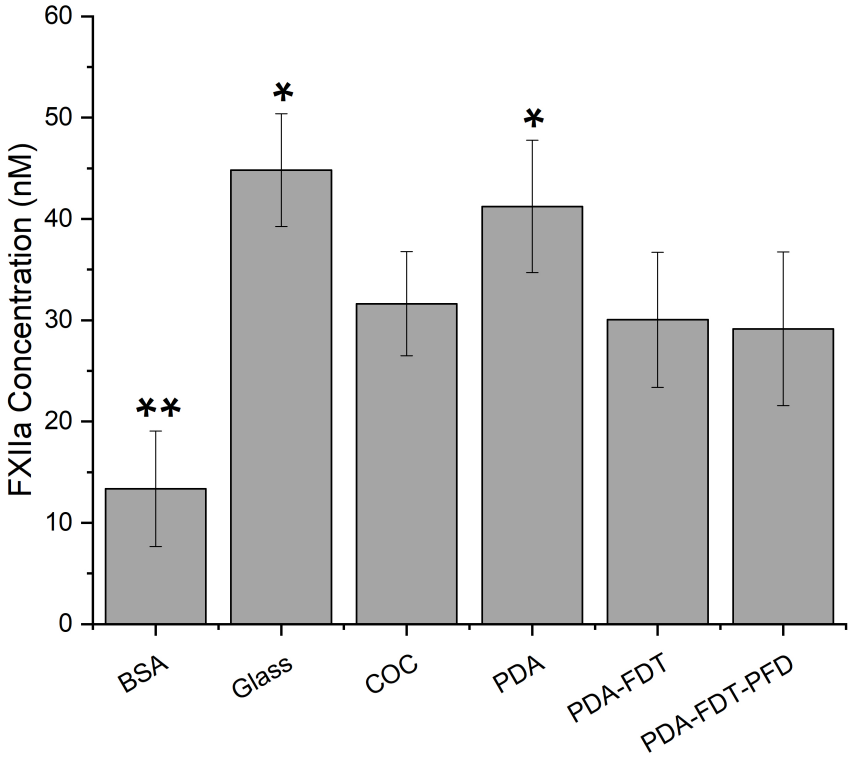

Figure 3.3. FXIIa concentration after 1 hour incubation with HMWK and PK on surfaces. Error bars indicate standard deviation, n = 18. COC, PDA-FDT and PDA-FDT-PFD activated 50% less FXII than PDA and glass, but 100% more than BSA. Single asterisk (*) and double asterisk (**) indicate significantly higher or lower activation, respectively ($\alpha = 0.05$).

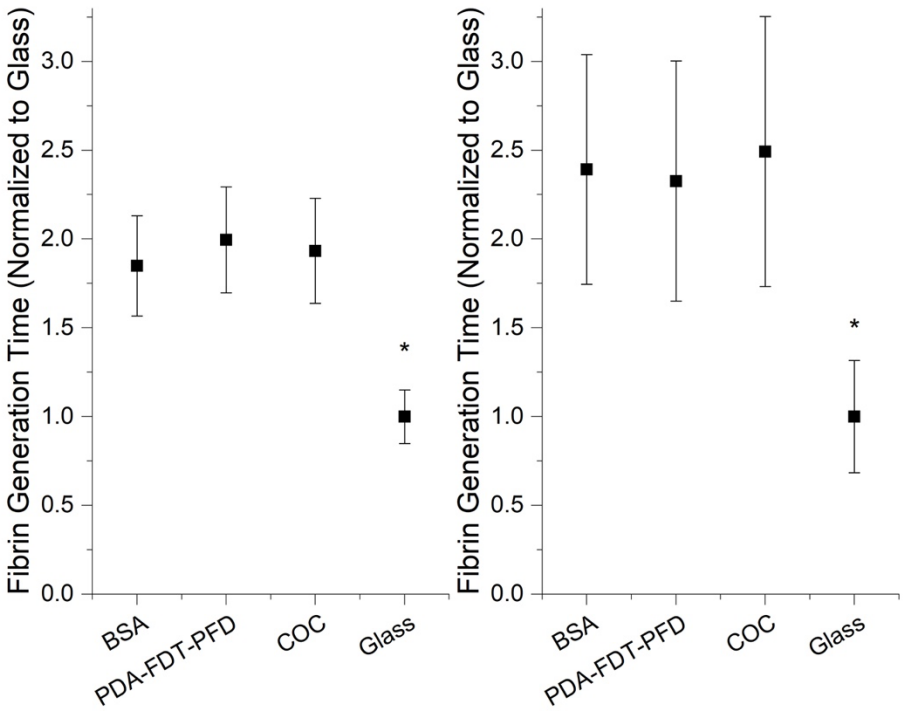

Figure 3.4. Fibrin generation time on modified surfaces for two donors, A1 (left) and A3 (right). Data was normalized to glass and combined for three runs. Error bars represent standard deviation. Recalcified citrated plasma was incubated with surfaces at 37ºC. OD was measured every 1 minute for 60 minutes. PPP clotted approximately 2.5x slower on PDA-FDT-PFD than glass for all runs and there was no difference between PDA-FDT-PFD and BSA or COC. Fibrin generation time was defined as the time to reach a 5% increase in OD over the baseline. PDA-FDT-PFD clotted significantly slower than glass for both donors and all runs ($\alpha = 0.05$).

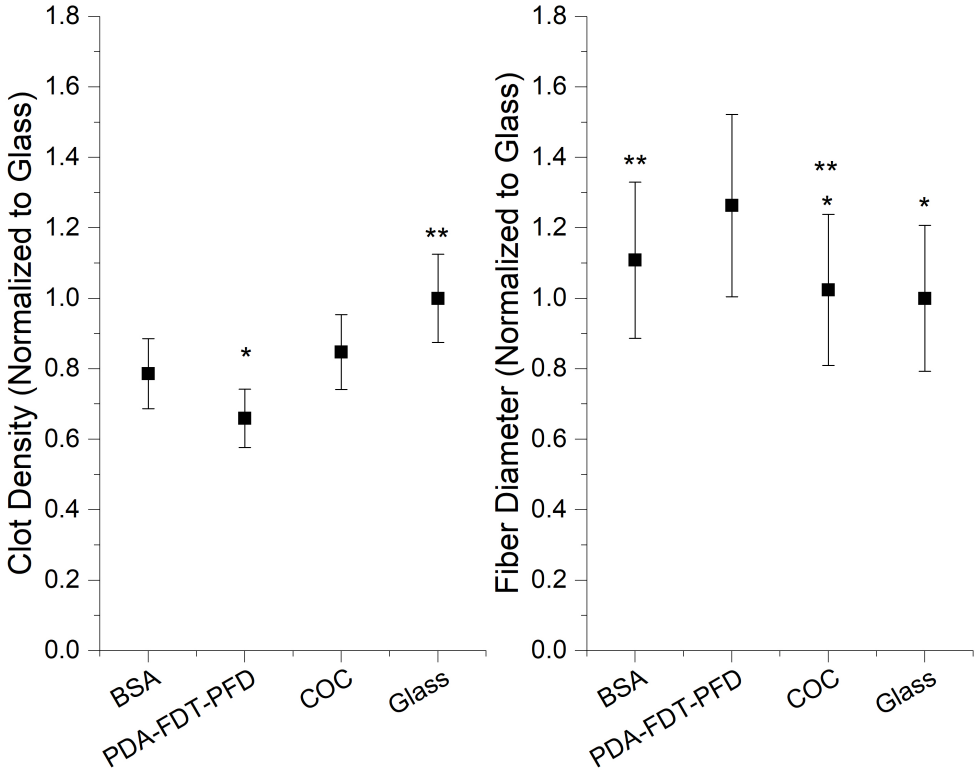

Figure 3.5. Clot morphology assessed using SEM after incubation of recalcified PPP on surfaces. Data are from a single donor. (Left) Fiber diameter, measured from 10 fibers (n = 60). (Right) Clot density, defined as the number of times a fiber crosses a line of fixed length. 3 lines were drawn per spot (n = 18). PDA-FDT-PFD had significantly higher fiber diameter and lower clot density than glass, COC and BSA ($\alpha = 0.05$).

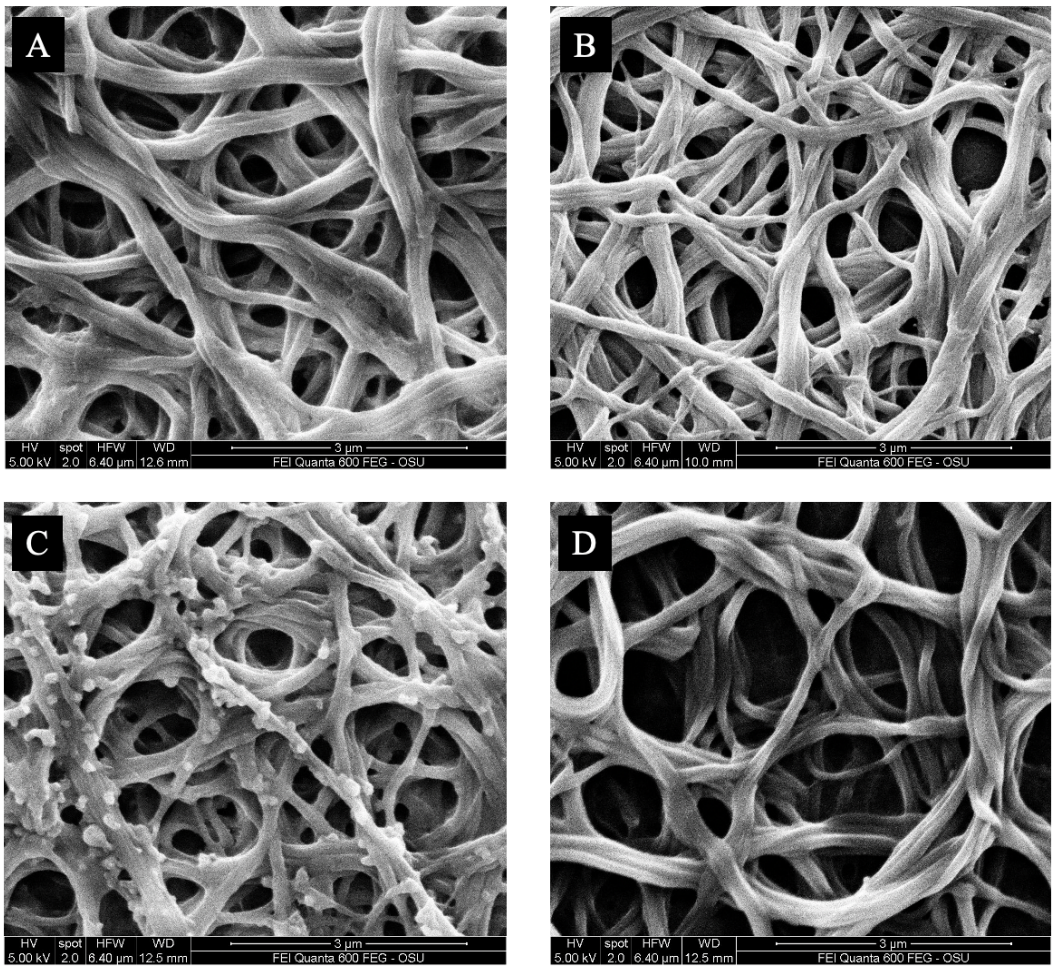

Figure 3.6. Representative SEM micrographs of clotted plasma on (A) BSA, (B) glass, (C) COC, and (D) PDA-FDT-PFD. Recalcified citrated PPP was incubated with surfaces for at least 10x the clotting time. All micrographs are from donor A1 run 1.

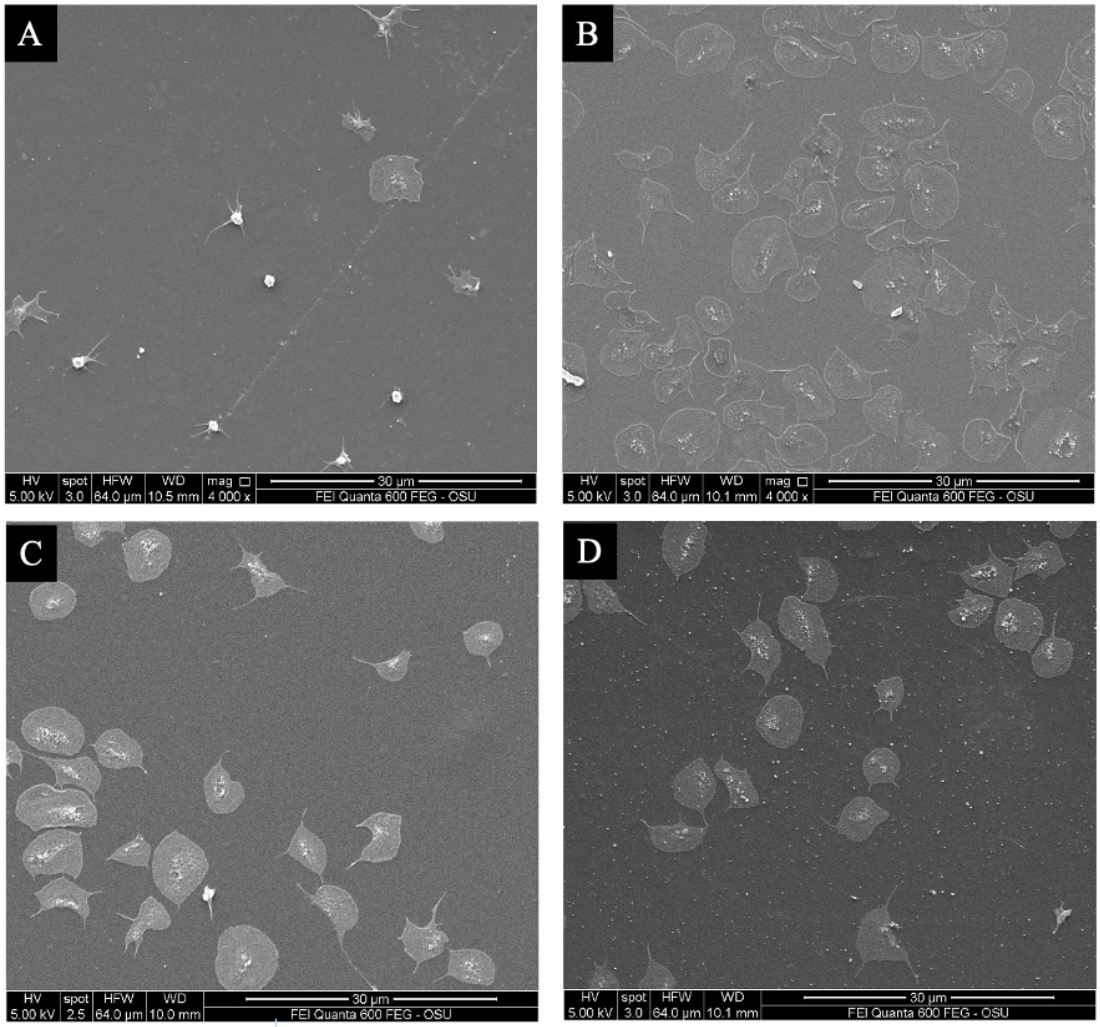

Figure 3.7. Representative SEM micrographs of adherent platelets on (A) BSA, (B) glass, (C) COC, and (D) PDA-FDT-PFD. Surfaces were incubated with 10^8 platelets/mL in Tyrode's buffer for 90 minutes.

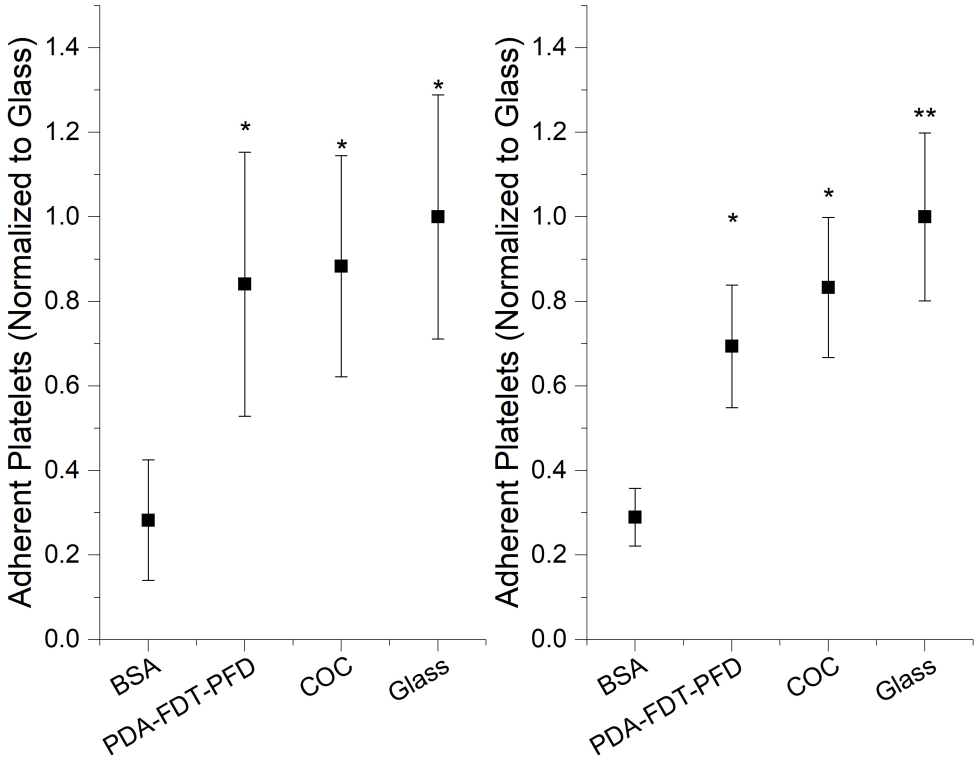

Figure 3.8. Adherent platelets per 3520 μm^2 surface area for two donors, A1 (left) and A3 (right). Surfaces were incubated with 10^8 platelets/mL in Tyrode's buffer for 90 minutes. Platelets were counted using SEM. For each donor and each run, 2 samples per sample group and 3 spots per sample were imaged. There was approximately 150% lower adhesion to BSA coated surfaces than all other groups. There was no difference in platelet adhesion between PDA-FDT-PFD, COC and glass for donor A1 and glass had significantly higher platelet adhesion than PDA-FDT-PFD and COC for donor A3.

Chapter 4 – Future Directions

4.1 Development of Flow Model

Blood-contacting medical devices such as extracorporeal circulation units, indwelling devices and delivery systems are subject to shear stress because of flow. While static test methods are a powerful first screening method, flow models are required to verify and validate a novel coating if the intended use is for a device subjected to flow [1, 2, 3]. A dynamic flow model is currently in development as part of to study the blood-contacting behavior of surfaces under physiological conditions. The model is based off of the Chandler Loop test system, which is an approved test method according to ISO 10994-4 [1]. Preliminary dynamic testing has been done on the bioinspired PDA SLIPS coating described in Chapter 3 and clinical controls.

Our laboratory setup includes a sous vide, motor, wheels for tubing, water bath, and thermometer (Figure 4.1). The wheels were designed such that the tubing would fit around the outer diameter. Parameters were selected such that flow would remain in the laminar domain and approximate physiological flow conditions.

Limited trials have been performed thus far. Next steps include finalizing the flow model setup. When the flow model design is validated, it can be applied to assays for specific coagulation factors (FXIIa, thrombin, etc.) and platelet adhesion and activation studies in addition to whole blood clotting time.

4.2 References

1. "ISO 10993-4:2017," *ISO*. https://www.iso.org/cms/render/live/en/sites/isoorg/contents/data/standard/06/34/63448.html

2. K. N. J. Stevens, Y. B. J. Aldenhoff, F. H. van der Veen, J. G. Maessen, and L. H. Koole, "Bioengineering of Improved Biomaterials Coatings for Extracorporeal Circulation Requires Extended Observation of Blood-Biomaterial Interaction under Flow," *J Biomed Biotechnol*, vol. 2007, 2007, doi: 10.1155/2007/29464.

3. U. T. Seyfert, V. Biehl, and J. Schenk, "In vitro hemocompatibility testing of biomaterials according to the ISO 10993-4," *Biomolecular Engineering*, vol. 19, no. 2, pp. 91–96, Aug. 2002, doi: 10.1016/S1389-0344(02)00015-1.

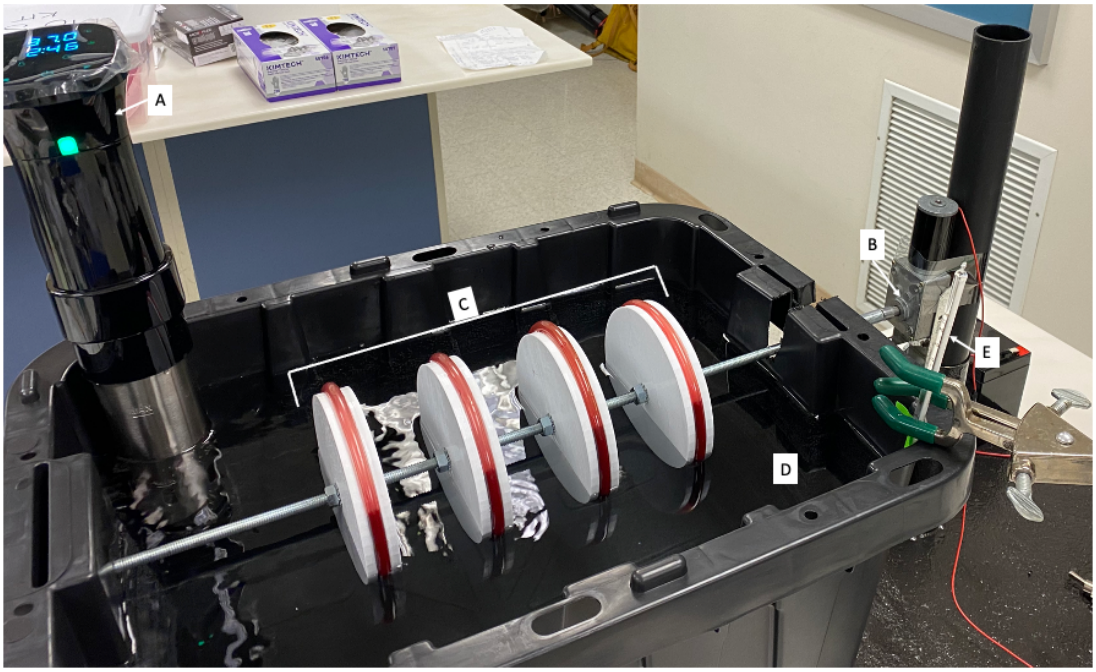

Figure 4.1. Laboratory setup of flow model. (A) Sous vide for temperature control. (B) Motor to spin threaded rod at 4rpm. (C) Wheels with tubing and whole blood. (D) Water bath at 37° C. (E) Thermometer to confirm temperature.

Bibliography

"ISO 10993-4:2017," *ISO*. https://www.iso.org/cms/render/live/en/sites/isoorg/contents/data/standard/06/34/63448.html

J. Bäck, J. Sanchez, G. Elgue, K. N. Ekdahl, and B. Nilsson, "Activated human platelets induce factor XIIa-mediated contact activation," *Biochemical and Biophysical Research Communications*, vol. 391, no. 1, pp. 11–17, Jan. 2010, doi: 10.1016/j.bbrc.2009.10.123.

M. Badv, I. H. Jaffer, J. I. Weitz, and T. F. Didar, "An omniphobic lubricant-infused coating produced by chemical vapor deposition of hydrophobic organosilanes attenuates clotting on catheter surfaces," *Scientific Reports (Nature Publisher Group)*, vol. 7, pp. 1–10, Sep. 2017, doi: http://dx.doi.org.ezproxy.proxy.library.oregonstate.edu/10.1038/s41598-017-12149-1.

N. M. Bates, C. Puy, P. L. Jurney, O. J. T. McCarty, and M. T. Hinds, "Evaluation of the Effect of Crosslinking Method of Poly(Vinyl Alcohol) Hydrogels on Thrombogenicity," *Cardiovasc Eng Tech*, vol. 11, no. 4, pp. 448–455, Aug. 2020, doi: 10.1007/s13239-020-00474-y.

U. Bauer and W. Federle, "The insect-trapping rim of Nepenthes pitchers," *Plant Signal Behav*, vol. 4, no. 11, pp. 1019–1023, Nov. 2009.

P. Bellavite *et al.*, "A colorimetric method for the measurement of platelet adhesion in microtiter plates," *Anal Biochem*, vol. 216, no. 2, pp. 444–450, Feb. 1994, doi: 10.1006/abio.1994.1066.

P. Blair and R. Flaumenhaft, "Platelet α–granules: Basic biology and clinical correlates," *Blood Rev*, vol. 23, no. 4, pp. 177–189, Jul. 2009, doi: 10.1016/j.blre.2009.04.001.

L. Bordenave, M. Rémy-Zolghadri, P. Fernandez, R. Bareille, and D. Midy, "Clinical performance of vascular grafts lined with endothelial cells," *Endothelium*, vol. 6, no. 4, pp. 267–275, 1999, doi: 10.3109/10623329909078494.

N. Bujandric and J. Grujic, "Exchange Transfusion for Severe Neonatal Hyperbilirubinemia: 17 Years' Experience from Vojvodina, Serbia," *Indian J Hematol Blood Transfus*, vol. 32, no. 2, pp. 208–214, Jun. 2016, doi: 10.1007/s12288-015-0534-1.

N. Capková *et al.*, “The Effects of Bilirubin and Lumirubin on the Differentiation of Human Pluripotent Cell-Derived Neural Stem Cells,” *Antioxidants (Basel)*, vol. 10, no. 10, p. 1532, Sep. 2021, doi: 10.3390/antiox10101532.

R. Carrell, R. Skinner, M. Wardell, and J. Whisstock, “Antithrombin and heparin,” *Molecular Medicine Today*, vol. 1, no. 5, pp. 226–231, Aug. 1995, doi: 10.1016/S1357-4310(95)91494-3.

Y. Chang, W.-J. Chang, Y.-J. Shih, T.-C. Wei, and G.-H. Hsiue, “Zwitterionic Sulfobetaine-Grafted Poly(vinylidene fluoride) Membrane with Highly Effective Blood Compatibility via Atmospheric Plasma-Induced Surface Copolymerization,” *ACS Appl. Mater. Interfaces*, vol. 3, no. 4, pp. 1228–1237, Apr. 2011, doi: 10.1021/am200055k.

R. E. Cronin and R. F. Reilly, “Unfractionated Heparin for Hemodialysis: Still the Best Option: UNFRACTIONATED HEPARIN FOR HEMODIALYSIS,” *Seminars in Dialysis*, vol. 23, no. 5, pp. 510–515, Sep. 2010, doi: 10.1111/j.1525-139X.2010.00770.x.

K. D. Curwen, H. Y. Kim, M. Vazquez, R. I. Handin, and M. A. Gimbrone, “Platelet adhesion to cultured vascular endothelial cells. A quantitative monolayer adhesion assay,” *J Lab Clin Med*, vol. 100, no. 3, pp. 425–436, Sep. 1982.

R. A. Faase, “Spherical Au Nanoparticle Interaction with Lipid Monolayers Probed with Sum Frequency Generation Spectroscopy.”

J. L. Fitch-Tewfik and R. Flaumenhaft, “Platelet Granule Exocytosis: A Comparison with Chromaffin Cells,” *Front Endocrinol (Lausanne)*, vol. 4, Jun. 2013, doi: 10.3389/fendo.2013.00077.

M. M. Flanders, R. Crist, and G. M. Rodgers, “Comparison of Five Thrombin Time Reagents,” *Clin Chem*, vol. 49, no. 1, pp. 169–172, Jan. 2003, doi: 10.1373/49.1.169.

M. M. Frojmovic and J. G. Milton, “Human platelet size, shape, and related functions in health and disease.,” *Physiological Reviews*, vol. 62, no. 1, pp. 185–261, Jan. 1982, doi: 10.1152/physrev.1982.62.1.185.

S. L. Goodman, “Sheep, pig, and human platelet-material interactions with model cardiovascular biomaterials,” *J Biomed Mater Res*, vol. 45, no. 3, pp. 240–250, Jun. 1999, doi: 10.1002/(sici)1097-4636(19990605)45:3<240::aid-jbm12>3.0.co;2-c.

E. L. Hethershaw *et al.*, “The effect of blood coagulation factor XIII on fibrin clot structure and fibrinolysis,” *Journal of Thrombosis and Haemostasis*, vol. 12, no. 2, pp. 197–205, 2014, doi: https://doi.org/10.1111/jth.12455.

T. A. Horbett, “Fibrinogen adsorption to biomaterials,” *J Biomed Mater Res A*, vol. 106, no. 10, pp. 2777–2788, Oct. 2018, doi: 10.1002/jbm.a.36460.

T. A. Horbett and P. K. Weathersby, “Adsorption of proteins from plasma to a series of hydrophilic-hydrophobic copolymers. I. Analysis with the in situ radioiodination technique,” *Journal of Biomedical Materials Research*, vol. 15, no. 3, pp. 403–423, 1981, doi: 10.1002/jbm.820150311.

C. Howell, A. Grinthal, S. Sunny, M. Aizenberg, and J. Aizenberg, “Designing Liquid-Infused Surfaces for Medical Applications: A Review,” *Advanced Materials*, vol. 30, no. 50, p. 1802724, 2018, doi: https://doi.org/10.1002/adma.201802724.

K. Ishihara, T. Ueda, and N. Nakabayashi, “Preparation of Phospholipid Polymers and Their Properties as Polymer Hydrogel Membranes,” *Polymer Journal*, vol. 22, no. 5, Art. no. 5, May 1990, doi: 10.1295/polymj.22.355.

L. Jin, J. P. Abrahams, R. Skinner, M. Petitou, R. N. Pike, and R. W. Carrell, “The anticoagulant activation of antithrombin by heparin,” *Proc Natl Acad Sci U S A*, vol. 94, no. 26, pp. 14683–14688, Dec. 1997.

A. H. Kamal, A. Tefferi, and R. K. Pruthi, “How to interpret and pursue an abnormal prothrombin time, activated partial thromboplastin time, and bleeding time in adults,” *Mayo Clinic Proceedings*, vol. 82, no. 7, pp. 864-, Jul. 2007.

R. Khalifehzadeh, W. Ciridon, and B. D. Ratner, “Surface fluorination of polylactide as a path to improve platelet associated hemocompatibility,” *Acta Biomaterialia*, vol. 78, pp. 23–35, Sep. 2018, doi: 10.1016/j.actbio.2018.07.042.

G. Lamour *et al.*, “Contact Angle Measurements Using a Simplified Experimental Setup,” *J. Chem. Educ.*, vol. 87, no. 12, pp. 1403–1407, Dec. 2010, doi: 10.1021/ed100468u.

H. Lee, S. M. Dellatore, W. M. Miller, and P. B. Messersmith, “Mussel-Inspired Surface Chemistry for Multifunctional Coatings,” *Science*, vol. 318, no. 5849, pp. 426–430, Oct. 2007, doi: 10.1126/science.1147241.

D. C. Leslie *et al.*, “A bioinspired omniphobic surface coating on medical devices prevents thrombosis and biofouling,” *Nature Biotechnology*, vol. 32, no. 11, Art. no. 11, Nov. 2014, doi: 10.1038/nbt.3020.

C.-Y. Liu and C.-J. Huang, “Functionalization of Polydopamine via the Aza-Michael Reaction for Antimicrobial Interfaces,” *Langmuir*, vol. 32, no. 19, pp. 5019–5028, May 2016, doi: 10.1021/acs.langmuir.6b00990.

P.-S. Liu *et al.*, “Grafting of Zwitterion from Cellulose Membranes via ATRP for Improving Blood Compatibility,” *Biomacromolecules*, vol. 10, no. 10, pp. 2809–2816, Oct. 2009, doi: 10.1021/bm9006503.

X. Liu *et al.*, “Blood compatible materials: state of the art,” *J. Mater. Chem. B*, vol. 2, no. 35, pp. 5718–5738, Aug. 2014, doi: 10.1039/C4TB00881B.

K. Manabe, K.-H. Kyung, and S. Shiratori, “Biocompatible Slippery Fluid-Infused Films Composed of Chitosan and Alginate via Layer-by-Layer Self-Assembly and Their Antithrombogenicity,” *ACS Appl. Mater. Interfaces*, vol. 7, no. 8, pp. 4763–4771, Mar. 2015, doi: 10.1021/am508393n.

K. G. Mann, M. F. Whelihan, S. Butenas, and T. Orfeo, “Citrate anticoagulation and the dynamics of thrombin generation,” *Journal of Thrombosis and Haemostasis*, vol. 5, no. 10, pp. 2055–2061, 2007, doi: https://doi.org/10.1111/j.1538-7836.2007.02710.x.

W. Mäntele and E. Deniz, “UV–VIS absorption spectroscopy: Lambert-Beer reloaded,” *Spectrochimica Acta Part A: Molecular and Biomolecular Spectroscopy*, vol. 173, pp. 965–968, Feb. 2017, doi: 10.1016/j.saa.2016.09.037.

M. M. Markiewski, B. Nilsson, K. Nilsson Ekdahl, T. E. Mollnes, and J. D. Lambris, “Complement and coagulation: strangers or partners in crime?,” *Trends in Immunology*, vol. 28, no. 4, pp. 184–192, Apr. 2007, doi: 10.1016/j.it.2007.02.006.

O. J. T. McCarty *et al.*, “Rac1 Is Essential for Platelet Lamellipodia Formation and Aggregate Stability under Flow,” *J Biol Chem*, vol. 280, no. 47, pp. 39474–39484, Nov. 2005, doi: 10.1074/jbc.M504672200.

L. Ngashangva, V. Bachu, and P. Goswami, “Development of new methods for determination of bilirubin,” *Journal of Pharmaceutical and Biomedical Analysis*, vol. 162, pp. 272–285, Jan. 2019, doi: 10.1016/j.jpba.2018.09.034.

A. F. B. Omar and M. Z. B. MatJafri, “Turbidimeter Design and Analysis: A Review on Optical Fiber Sensors for the Measurement of Water Turbidity,” *Sensors (Basel)*, vol. 9, no. 10, pp. 8311–8335, Oct. 2009, doi: 10.3390/s91008311.

D. A. Palanzo *et al.*, “Effect of Carmeda BioActive Surface coating versus Trillium Biopassive Surface coating of the oxygenator on circulating platelet count drop during cardiopulmonary bypass,” *Perfusion*, vol. 16, no. 4, pp. 279–283, Jul. 2001, doi: 10.1177/026765910101600403.

C. Puy *et al.*, “Factor XII promotes blood coagulation independent of factor XI in the presence of long chain polyphosphate,” *J Thromb Haemost*, vol. 11, no. 7, pp. 1341–1352, Jul. 2013, doi: 10.1111/jth.12295.

J. E. Rothman and L. Orci, “Molecular dissection of the secretory pathway,” *Nature*, vol. 355, no. 6359, pp. 409–415, Jan. 1992, doi: 10.1038/355409a0.

K. N. Sask, W. G. McClung, L. R. Berry, A. K. C. Chan, and J. L. Brash, “Immobilization of an antithrombin–heparin complex on gold: Anticoagulant properties and platelet interactions,” *Acta Biomaterialia*, vol. 7, no. 5, pp. 2029–2034, May 2011, doi: 10.1016/j.actbio.2011.01.031.

M. Schapira *et al.*, “High molecular weight kininogen or its light chain protects human plasma kallikrein from inactivation by plasma protease inhibitors,” *Biochemistry*, vol. 21, no. 3, pp. 567–572, Feb. 1982, doi: 10.1021/bi00532a024.

U. T. Seyfert, V. Biehl, and J. Schenk, “In vitro hemocompatibility testing of biomaterials according to the ISO 10993-4,” *Biomolecular Engineering*, vol. 19, no. 2, pp. 91–96, Aug. 2002, doi: 10.1016/S1389-0344(02)00015-1.

S. A. Smith and J. H. Morrissey, “Polyphosphate enhances fibrin clot structure,” *Blood*, vol. 112, no. 7, pp. 2810–2816, Oct. 2008, doi: 10.1182/blood-2008-03-145755.

C. Sperling, M. Fischer, M. F. Maitz, and C. Werner, “Blood coagulation on biomaterials requires the combination of distinct activation processes,” *Biomaterials*, vol. 30, no. 27, pp. 4447–4456, Sep. 2009, doi: 10.1016/j.biomaterials.2009.05.044.

E. Stavrou and A. H. Schmaier, “Factor XII: What Does It Contribute To Our Understanding Of The Physiology and Pathophysiology of Hemostasis & Thrombosis,” *Thromb Res*, vol. 125, no. 3, pp. 210–215, Mar. 2010, doi: 10.1016/j.thromres.2009.11.028.

K. N. J. Stevens, Y. B. J. Aldenhoff, F. H. van der Veen, J. G. Maessen, and L. H. Koole, “Bioengineering of Improved Biomaterials Coatings for Extracorporeal Circulation Requires Extended Observation of Blood-Biomaterial Interaction under Flow,” *J Biomed Biotechnol*, vol. 2007, 2007, doi: 10.1155/2007/29464.

L. J. Suggs, J. L. West, and A. G. Mikos, “Platelet adhesion on a bioresorbable poly(propylene fumarate-co-ethylene glycol) copolymer,” *Biomaterials*, vol. 20, no. 7, pp. 683–690, Apr. 1999, doi: 10.1016/s0142-9612(98)00226-9.

D. F. Swinehart, “The Beer-Lambert Law,” p. 3.

L. M. Szott, M. J. Stein, B. D. Ratner, and T. A. Horbett, “Complement activation on poly(ethylene oxide)-like RFGD-deposited surfaces,” *J Biomed Mater Res A*, vol. 96, no. 1, pp. 150–161, Jan. 2011, doi: 10.1002/jbm.a.32954.

Y. Tamada, E. A. Kulik, and Y. Ikada, “Simple method for platelet counting,” *Biomaterials*, vol. 16, no. 3, pp. 259–261, Feb. 1995, doi: 10.1016/0142-9612(95)92126-q.

A. S. Thiara *et al.*, “Comparable biocompatibility of Phisio- and Bioline-coated cardiopulmonary bypass circuits indicated by the inflammatory response,” *Perfusion*, vol. 25, no. 1, pp. 9–16, Jan. 2010, doi: 10.1177/0267659110362822.

S. ULLAH, K. RAHMAN, and M. HEDAYATI, “Hyperbilirubinemia in Neonates: Types, Causes, Clinical Examinations, Preventive Measures and Treatments: A Narrative Review Article,” *Iran J Public Health*, vol. 45, no. 5, pp. 558–568, May 2016.

M. Vaníčková, J. Suttnar, and J. E. Dyr, “The adhesion of blood platelets on fibrinogen surface: Comparison of two biochemical microplate assays,” *Platelets*, vol. 17, no. 7, pp. 470–476, Nov. 2006, doi: 10.1080/09537100600758875.

J. Wang, G. Guo, A. Li, W.-Q. Cai, and X. Wang, “Challenges of phototherapy for neonatal hyperbilirubinemia (Review),” *Experimental and Therapeutic Medicine*, vol. 21, no. 3, pp. 1–1, Mar. 2021, doi: 10.3892/etm.2021.9662.

M. Weber *et al.*, “Blood-Contacting Biomaterials: In Vitro Evaluation of the Hemocompatibility,” *Front Bioeng Biotechnol*, vol. 6, Jul. 2018, doi: 10.3389/fbioe.2018.00099.

J. W. Weisel and C. Nagaswami, “Computer modeling of fibrin polymerization kinetics correlated with electron microscope and turbidity observations: clot structure and assembly are kinetically controlled.,” *Biophys J*, vol. 63, no. 1, pp. 111–128, Jul. 1992.

J. G. White and C. C. Clawson, “The surface-connected canalicular system of blood platelets--a fenestrated membrane system.,” *Am J Pathol*, vol. 101, no. 2, pp. 353–364, Nov. 1980.

T.-S. Wong *et al.*, “Bioinspired self-repairing slippery surfaces with pressure-stable omniphobicity,” *Nature*, vol. 477, no. 7365, Art. no. 7365, Sep. 2011, doi: 10.1038/nature10447.

L.-C. Xu, J. W. Bauer, and C. A. Siedlecki, “Proteins, platelets, and blood coagulation at biomaterial interfaces,” *Colloids and Surfaces B: Biointerfaces*, vol. 124, pp. 49–68, Dec. 2014, doi: 10.1016/j.colsurfb.2014.09.040.

S. Yuan, S. Luan, S. Yan, H. Shi, and J. Yin, “Facile Fabrication of Lubricant-Infused Wrinkling Surface for Preventing Thrombus Formation and Infection,” *ACS Appl. Mater. Interfaces*, vol. 7, no. 34, pp. 19466–19473, Sep. 2015, doi: 10.1021/acsami.5b05865.

R. Zhuo, C. A. Siedlecki, and E. A. Vogler, “Autoactivation of blood factor XII at hydrophilic and hydrophobic surfaces,” *Biomaterials*, vol. 27, no. 24, pp. 4325–4332, Aug. 2006, doi: 10.1016/j.biomaterials.2006.04.001.

“SNAP receptors implicated in vesicle targeting and fusion | Nature.” https://www.nature.com/articles/362318a0 (accessed Nov. 18, 2021).

Appendices

Appendix A – MATLAB Code for Determining FXIIa Concentration

```
%% FXIIa.m
%FXIIa.m takes inputs of a numeric matrix of absorbance data and a
%string array of variable names and outputs plots of data with
linear
%regression line and table of rate of color change (rate_FXIIa)

%import data as numeric matrix, name 'data'
%import sample names as separate string array, name 'names'
%define time vector
t = data(:,1);
lx = 5;     %where to start fitting data
hx = 26;    %where to stop fitting data

for i = 1:width(data)
    [fit(:,i),S(:,i)] = polyfit(t(lx:hx),data(lx:hx,i),1);
    [y_fit(:,i),error(:,i)] = polyval(fit(:,i),t(lx:hx),S(:,i));
    figure
    plot(t(lx:hx),data(lx:hx,i),'bo')
    hold on
    plot(t(lx:hx),y_fit(:,i),'r-')
    xlabel('Time (min)')
    ylabel('OD')
    title(names(i))
    hold off
end

%assign rates to sample names
rate_FXIIa(1,:) = table(names);
rate_FXIIa(2,:) = table(fit(1,:));
```

Appendix B – MATLAB Code for Determining Fibrin Generation Time

```
%% Fibrin generation method comparison
%this section computes fibrin generation time as time to reach a 5%
%increase over baseline OD

%define time vector
t = data(:,1);

%define time step
dt = (t(end)-t(1))/(length(t)-1);

%predefine derivative vector
abs_dt = zeros(height(data),width(data));

%calculate derivative and threshold
for i = 1:width(data)   %iterate through columns (samples)
    for j = 2:height(data)-1    %iterate through rows (time points)
        abs_dt(j,i) = (data(j+1,i) - data(j-1,i))/(2*dt);
%calculate derivative
    end
    threshold(i) = 1.05*mean(data(2:10,i));  %calculate 5% increase
threshold
    [rate_val,I] = max(abs_dt(5:end,:));  %define rate as maximum
change in OD
end

%predefine threshold crossing vector
cross = 2*ones(1,width(data));

%find where data crosses threshold
for i = 1:width(data)   %iterate through columns (samples)
    for j = 1:height(data)  %iterate through rows (time points)
        if data(j,i) < threshold(i) %if data point below threshold,
move to next
            j = j+1;
        else
            cross(i) = j;   %if data crosses threshold, populate
vector and break
            break
        end
    end
end

%predefine interpolation vectors
x = zeros(2, width(data));
v = zeros(2, width(data));
xq = zeros(60, width(data));
vq = zeros(60, width(data));
```

```
for i = 2:width(data)   %iterate through columns (samples)
    x(:,i) = (cross(i)-1:cross(i))';    %populate array with time
point before and after crossing
    v(:,i) = data(cross(i)-1:cross(i),i);   %populate array with OD
before and after crossing
end

for i = 2:width(data)   %iterate through columns (samples)
    xq(:,i) = linspace(cross(i)-1,cross(i),60); %define queary time
points
    vq(:,i) = (interp1(x(:,i),v(:,i),xq(:,i))); %interpolate OD
values for queary points
end

%redefine variables
time_inter = xq;
OD_inter = vq;

%predefine vectors
OD_cross = zeros(1, width(data));
gen_time_val = zeros(1, width(data));

%find time from interpolation where data crosses threshold
for i = 1:width(time_inter)     %iterate through columns (samples)
    for j = 1:height(time_inter)    %iterate through rows (time
points)
        if OD_inter(j,i) < threshold(i)
            j = j+1;
        else
            gen_time_val(i) = (time_inter(j,i)-1);  %populate vector
with time of threshold cross
            OD_cross(i) = OD_inter(j,i);    %populate vector with
corresponding OD
            break
        end
    end
end

%assign fibrin generation times to sample names
gen_time(1,:) = table(names);
gen_time(2,:) = table(gen_time_val);

%plot data, threshold, and interpolated generation time
for i = 1:width(data)
    figure
    plot(t,data(:,i),'linewidth',2)
    hold on
    plot(gen_time_val(i),OD_cross(i),'k*')
    yline(threshold(i));
    xlabel('Time (min)')
    ylabel('OD')
    title(names(i))
```

```
    hold off
end
```